GEOLOGICA BELGICA (2013) 16/1-2: 001-017

Brittle tectonic and stress field evolution in the Pan-African Lufilian arc and its foreland (Katanga, DRC): from orogenic compression to extensional collapse, transpressional inversion and transition to rifting.

Mwabanwa Louis KIPATA[1,2,3], Damien DELVAUX[3,4], Mwene Ntabwoba SEBAGENZI[2], Jacques CAILTEUX,[5] & Manuel SINTUBIN[1]

[1] *Geodynamics and Geofluids Research Group, K.U.Leuven, Celestijnenlaan 200E, B-3001, Leuven, Belgium*
[2] *Department of Geology, University of Lubumbashi, Route Kasapa, Lubumbashi, DRC*
[3] *Royal Museum of Central Africa, Leuvensesteenweg 13, B-3080, Tervuren, Belgium*
[4] *School of Geosciences, University of the Witwatersrand, Johannesburg, 2050 Wits, South Africa*
[5] *Department of Research and Development, Forrest Group, 22 Av. Kigoma, Lubumbashi, DRC*

ABSTRACT. Since the first and paroxysmal deformation stages of the Lufilian orogeny at ~ 550 Ma and the late Neogene to Quaternary development of the south-western branch of the East African rift system, the tectonic evolution of the Lufilian arc and Kundelungu foreland in the Katanga region of the Democratic Republic of Congo remains poorly known although it caused important Cu-dominated mineral remobilizations leading to world-class ore deposits. This long period is essentially characterized by brittle tectonic deformations that have been investigated by field studies in open mines spread over the entire arc and foreland. Paleostress tensors were computed for a database of 1889 fault-slip data by interactive stress tensor inversion and data subset separation. They have been assembled and correlated into 8 major brittle events, their relative succession established primarily from field-based criteria and interpreted in function of the regional tectonic context. The first brittle structures observed were formed during the Lufilian compressional climax, after the transition from ductile to brittle deformation (stage 1). They have been re-oriented during the orogenic bending that led to the arcuate shape of the belt (stage 2). Unfolding the stress directions allows to reconstruct a well-defined N-S to NNE-SSW direction of compression, consistent with the stress directions recorded outside the belt. Constrictional deformation occurred in the central part of the arc, probably during orogenic bending. After the bending, the Lufilian arc was affected by a NE-SW transpression of regional significance (stage 3), inducing strike-slip reactivations dominantly sinistral in the Lufilian arc and dextral in the Kundelungu foreland. The next two stages were recorded only in the Lufilian arc. Late-orogenic extension was induced by $\sigma1$–$\sigma3$ stress axis permutation in a more trans-tensional regime (stages 4). Arc-parallel extension (stage 5) marks the final extensional collapse of the Lufilian orogeny. In early Mesozoic, NW-SE transpressional inversion felt regionally (stage 6) was induced by far-field stresses generated at the southern active margin of Gondwana. Since then, this region was affected by rift-related extension, successively in a NE-SW direction (stage 7, Tanganyika trend) and NW-SE direction (stage 8, Moero-Upemba trend).

KEYWORDS: brittle structural evolution, paleostress tensor, orogenic bending, extension, inversion, rifting

1. Introduction

The Lufilian arc is one of the Pan-African orogenic belt in south-central Africa (Fig. 1, insert), besides the Mozambique, Lurio, Zambezi, Damara and West-Congolian belts (Frimmel et al., 2006, 2011; Porada & Behorst, 2000; Viola et al., 2008). It deforms the Neoproterozoic Katangan sedimentary series in southeast D.R.Congo and Zambia in a fold-and thrust belt with large tectonic breccias and abundant brittle deformation structures (François, 1987, 1993, 2006; Cailteux & Kampunzu, 1995; Kampunzu & Cailteux, 1999; Jackson et al., 2003; Wendorff, 2011). Unlike the other Pan-African belts, it is a bent orogen and hosts world class Cu-Co mineral deposits (i.e. Copper belt). The latter are either stratiform deposits or are associated to faults systems (Robert, 1956; Mendelsohn, 1961; Oosterbosch, 1962; Cailteux et al., 2005b; Dewaele et al., 2006; Muchez et al., 2008; Haest et al., 2009; Kampunzu et al., 2009; El Desouky et al., 2010).

The Lufilian arc, its Kundelungu foreland and adjacent Kibaran belt are presently undergoing continental extension and are involved in the poorly defined SW branch of the East African Rift System (Sebagenzi and Kaputo, 2002; Kipata, 2007). The present-day stress field is extensional as determined from the inversion of earthquake focal mechanisms (Delvaux & Barth,

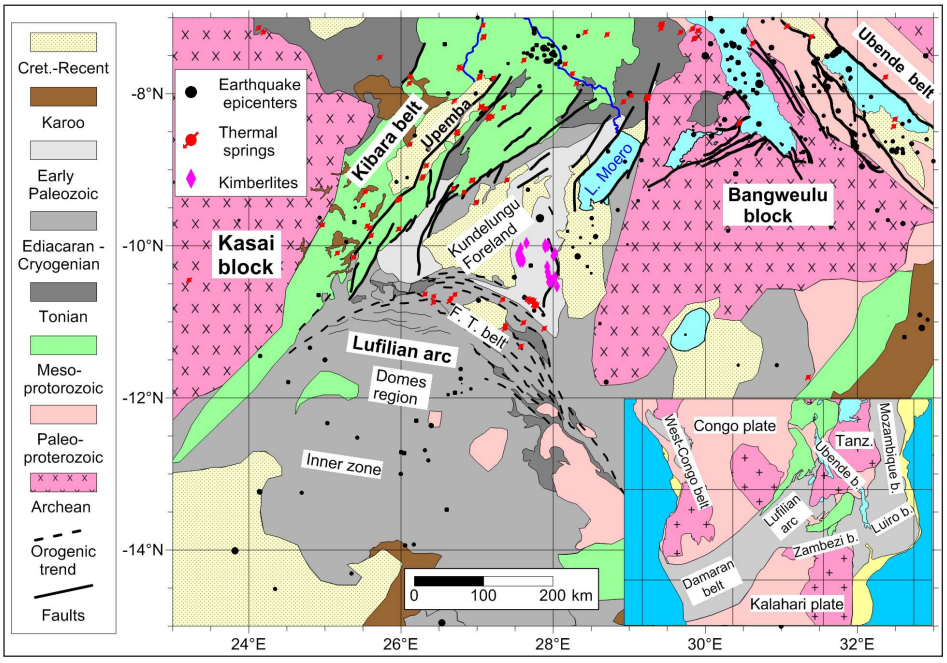

Figure 1. Geological and tectonic framework of the Lufilian arc, Kundelungu foreland and Kibaran belt and surrounding regions with structural subdivisions of the Lufilian arc (after Kampunzu & Cailteux, 1999), location of Eocene-Oligocene Kimberlite pipes in the Kundelungu plateau (Batumike et al., 2008), thermal springs (Robert, 1956) and seismic epicentres (USGS, IRIS and South African catalogs). Insert showing Neoproterozoic belts in south-central Africa and major crustal plates.

2010). Between the early tectonic stages of the Lufilian orogeny and the recent to still active rift-related crustal extension, little is known for this ~ 550 Ma long tectonic evolution which occurred mainly in brittle regime. If the general tectonic evolution of the Lufilian arc is relatively well documented by regional studies and mining exploration, the brittle faulting evolution has never been analyzed in detail although it is known that it contributed significantly to successive stages of mineral remobilizations and enrichments that led the mineral deposits.

This study aims at documenting the brittle deformation events that characterize the evolution of the Lufilian orogeny since the onset of the brittle realms, from the first recorded brittle compressional stage to the late extensional stages and the transition to the subsequent continental rifting. We performed kinematic analysis of brittle tectonic structures (faults and fractures) in ancient and active mining open casts and occasional exposures, and reconstructed the stress state that generated or reactivated them using the Win-Tensor software (Delvaux & Sperner, 2003; Delvaux, 2012). The results are assembled into a series of stress stages, some of which correlated with other regional paleostress data. The brittle tectonic and stress evolution is discussed in the framework of the geodynamic history of Central Africa.

2. Geological Setting

The Lufilian arc (Fig. 1) is subdivided into three domains, the Fold-and-Thrust belt (Outer Lufilian), the Domes region (Middle-Lufilian) and the Synclinorial belt or Inner zone (Inner Lufilian) (De Swardt & Drysdall, 1964; De Swardt et al., 1965; Daly et al., 1984). The Inner-Lufilian is entirely located in Zambia. The Middle Lufilian is slightly exposed in the D.R.Congo, along the Congo-Zambia border. The Kundelungu plateau represents the foreland of the Lufilian arc, squeezed between the Kibaran margin and the Bangweulu block.

Development of the Lufilian arc is linked to the amalgamation of the Gondwana Supercontinent in south-central and eastern Africa during the Pan-African orogeny (Grantham et al., 2003; De Waele et al., 2008; Westerhof et al., 2008). It formed, together with the Zambezi belt, during collision between the Congo and Kalahari cratons between 650-600 and 530 Ma, peaking at ~ 550 Ma and ending at ~ 530 Ma (Hanson et al., 1993; Porada & Behorst, 2000; John et al., 2004; Frimmel et al., 2011). In parallel, the evolution of the Lufilian arc was also influenced by closure of the Mozambique Ocean (840 - 630 Ma) and the collision of West and East Gondwana (640 - 530 Ma) which resulted in the formation of the East African – Antarctica orogen (Shackleton, 1994; Wilson, 1997; Kröner et al., 2001; Jacobs et al., 2008; Bingen et al., 2009). In NE Mozambique, the NE-trending Luiro belt formed under NW-SW compression (Viola et al., 2008) and could represent a major collisional suture zone between north and south Gondwana (Grantham et al., 2003). After ~530 Ma both the Luiro belt and the Dronning Maud land in East Antarctica underwent voluminous post-collisional magmatism and metamorphism (530 – 507 Ma, last manifestations until 485 Ma) together with extensional shearing in Dronning Maud (~ 507 Ma), evidencing extensional collapse of an overthickened crust (Jacobs et al., 2006; Bingen et al., 2009)

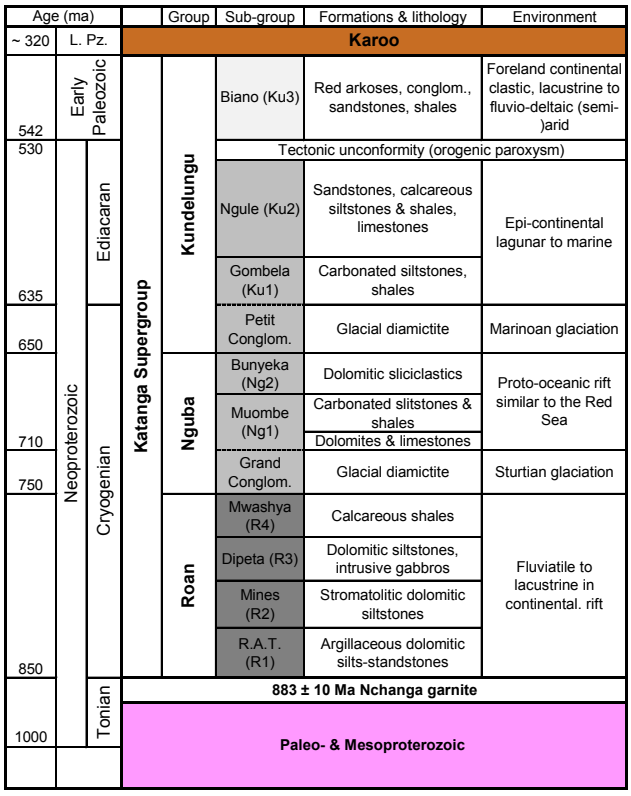

Figure 2. Simplified stratigraphy of the Lufilian arc, compiled from Cailteux et al. (2005a, 2005b, 2007) and Batumike et al. (2007). Units RSF (Roche siliceuse feuilletée), RSC (Roches siliceuse cellulaire), CMN (Calcaire à minéraux noirs) and SD (Shale dolomitique) are part of the Mines sub-group (R2).

The exposed region of the Katangan Supergroup is surrounded by the Archean - Paleoproterozoic Bangweulu block to the Southeast, the Paleoproterozoic Ubende belt to the East and the Mesoproterozoic Kibaran belt to the West (Fig. 1). To the north and north-west, the Katangan Supergroup overlies the Kibaran basement with a basal unconformity (Cahen, 1954; Kokonyangi et al., 2006; Batumike et al., 2007). The basement (Paleo- or Mesoproterozoic) is also exposed in the Inner- and Middle-Lufilian (Unrug, 1988). The Katanga Supergroup is believed to have been deposited in an extensional (rift) context with a thickness of 7 to 10 km (Cahen, 1954; Kampunzu & Cailteux, 1999). It is subdivided into Roan, Nguba and Kundelungu Groups (Fig. 2), separated by two well exposed diamictites / tillites of regional significance (Cailteux et al., 2005a): the Grand-conglomérat at the base of Nguba Group and the Petit-conglomérat (Kiandamu Formation) at the base of the Kundelungu Group. The Petit-conglomérat which contains clasts of the underlying Nguba Group marks the inversion from extensional to compressional tectonics and the onset of the north-verging Lufilian folding and thrusting (Batumike et al., 2007).

The Roan basin evolved from a continental rift through a proto-oceanic basin (Afar/Red Sea type) during the Rodinia Supercontinent break-up (Kampunzu et al., 1993, 2000; Meert & Van der Voo, 1997; Tembo et al., 1999; Batumike et al., 2007). The Roan Group consists of clastic deposits and carbonates, predominantly dolomites and dolomitic shales (Oosterbosch, 1962; François, 1987; Cailteux, 1994). The Nguba and Kundelungu Groups as well as the underlying upper Roan (Mwashya Subgroup, R4) consist of thick carbonate or siliciclastic sediments deposited in a broad basin (Cailteux et al., 2007). Their deposition is related to a major phase of extensional tectonics and normal faulting that mark the transition to a Red Sea-type proto-ocean (Buffard, 1988; Kampunzu et al., 1993).

Deformation in the Lufilian arc is expressed by north-verging folding and thrusting. The dominant structures observed are however NE-verging folds, thrust sheets and left-lateral strike-slip faults. The Lufilian belt has a northward convex arcuate shape, whose origin is still debated. Three major deformation phases have been observed (François, 1987; Kampunzu & Cailteux, 1999). The first stage (D1 or Kolwezian) corresponds to the major folding and thrusting with a northwards transport direction, together with along-trend higher angle forward and backward reverse faults. It gave the Lufilian belt the structure of a thin-skinned fault-and-thrust belt. Low-angle thrust faults formed in the RAT (Roches Argilo-Talqueuses, R1) and Dipeta (R3) Roan Subgroups, detaching the Roan from the basement (Cailteux & Kampunzu, 1995; Tshiauka et al., 1995; Cailteux et al., 2005a; Cailteux & Misi, 2007). Dewatering and fuidization of evaporite-bearing beds facilitated the dislocation, displacement and stacking of the Katangan tectonic sheets with formation of megabreccias which Roan fragments as large as 1 - 2 km (Cailteux & Kampunzu, 1995). Those have alternatively been interpreted as olistostromes (Wendorff, 2011).

The second stage (D2 or Monwezian) affected the folded and thrusted terranes by E-W sinistral strike-slip faulting in the western part of the belt (Monwezi fault system). These faults are frequently injected by fragments of the underlying

Roan sediments (extrusion faults of François, 1987) and some are associated to uranium-ore deposits as in Shinkolobwe. The bending of the arc is interpreted by Kampunzu & Cailteux (1999) as related to strike-slip tectonics of stage D2 due to the action of an indentor like for the India-Asia collision. The less well defined stage D3 (Shilatembo) is considered as responsible for orthogonal trending NE-SW open upright folds and conjugated, N160-170°E and N70-80°E in the eastern part of the belt, suggesting a NW-SE compression.

Stratiform and vein-type Cu-mineral deposits emplaced at different development stage of the orogen and fracture-controlled enrichments are also present in the foreland (Cailteux et al., 2005b; Dewaele et al., 2006; Cailteux & Misi, 2007; Muchez et al., 2008, 2010; El Desouky et al., 2009, 2010; Kampunzu et al., 2009; De Putter et al., 2010). The remobilizing mineralization stages have been related to the orogenic evolution (Haest & Muchez (2011). The first stratiform mineral deposits developed during the early diagenesis of the Roan formation, soon after its deposition in the early Neoproterozoic. New stratiform deposits formed by remobilisation related to the late diagenesis and the major thrusting and folding of the Lufilian orogenic stage (580 – 520 Ma). Vein-type deposits formed during the waning stage of the Lufilian orogeny (530 – 500 Ma). The Cu-dominated deposits were still remobilized in post-Lufilian times, with a young enrichment evidenced in the Kundelungu foreland at c. 100 Ma ago (Haest et al., 2010).

Long after the Lufilian orogeny, large subsiding tectonic basins developed in the Kibaran margin (Upemba depression) and the Kundelungu foreland (Moero graben), together with moderate seismicity (Calais et al., 2006; Craig et al., 2011) and thermo-mineral springs (Robert, 1956; Mondeguer et al., 1989; Sebagenzi & Kaputo, 2002; Kipata, 2007). The presence of Eocene-Oligocene (~ 32 Ma) Kimberlite pipes in the Kundelungu Plateau (Batumike et al., 2008) suggests that intracontinental extension was already active at that time. All this activity is interpreted to be indicative of the development of a NE-trending incipient rift branch, as a propagation of the East African Rift System (EARS) into southern Africa (Sebagenzi & Kaputo, 2002).

3. Brittle structural analysis and paleostress reconstruction

3.1 Fault-slip data collection

Fault-slip data (fault planes with associated slickenside lineation, tension and shear fractures) have been collected from a total of 22 new sites (Fig. 3), in the Lufilian arc (Kat01-04, 07-12, 16-19), the Kundelungu foreland (Kat05-06, 13) along the Kibaran margin (Kat14), at Manono inside the Kibaran belt (Kat21) and at Chishi Lake in the Bangweulu block in Zambia (DD801). They have been completed by existing data for the Dikulushi mine (Dik'shi) on the margin of Lake Moero (Haest & al., 2007; Haest, 2009) and by data from Kinsevere (Kat20) collected jointly by one of us (D. Delvaux) with B. Kazadi (Kazadi, 2012). All kind of fault and fractures that can be used as kinematic indicator in paleostress analysis (Petit, 1987; Angelier, 1994; Dunne & Hancock, 1994) have been measured and described: fault planes with slickenlines and slip sense (Fig. 4a-d), tension veins and plumose joints (Fig. 4e), shear fractures (Fig. 4f), conjugated shear fracture systems as well as shear planes with associated "en-echelon" tensile joints. Faults with slip line and slip sense best constrain the stress tensor, but the other types of fracture are also useful indicators as they provide additional although less complete constraints.

Additional qualitative parameters have been carefully recorded in the field in order to provide a complete description of the fault-slip data: the fault-rock type, cross-cutting relations, striae superposition (Fig. 4b), reactivations, associated mineral coating or host-rock mineralization (Fig. 4a), fracture dimension and confidence level in slip-sense determination. The fault-slip data have been classified into preliminary subsets according to their field characteristics and relative age estimation.

The geological structures in the studied region are well exposed in open pit mines but rarely in outcrops. The large size of the mines and their recent or active industrial and/or artisanal exploitation allowed collecting extensive data sets, often showing complex brittle histories with multistage evolution. Most of the sites offer a series of separated outcrops or sectors that have been studied separately as sub-sites. At each site or sub-site, the entire data set is further subdivided into subsets when multistage brittle history is observed.

3.2 Stress tensor determination

Geological fault-slip data can be used to reconstruct the 4 parameters of the reduced tectonic stress tensor assuming that slip on a plane occurs in the direction of maximum resolved shear stress (Wallace, 1951; Bott, 1959). These are the principal stress axes σ_1, σ_2, σ_3 with $\sigma_1 \geq \sigma_2 \geq \sigma_3 \geq 0$ and the ratio of principal stresses $R = (\sigma_2-\sigma_3) / (\sigma_1-\sigma_3)$ with $0 \leq R \leq 1$ (Angelier, 1989, 1994; Gephart & Forsyth, 1984; Vandycke & Bergerat, 1992).

Different techniques and computer programs packages (Carey's, Tector, MyFault, TectonicsFP, FaultKinWin, Win-Tensor, …) have been developed for fault-slip data analysis

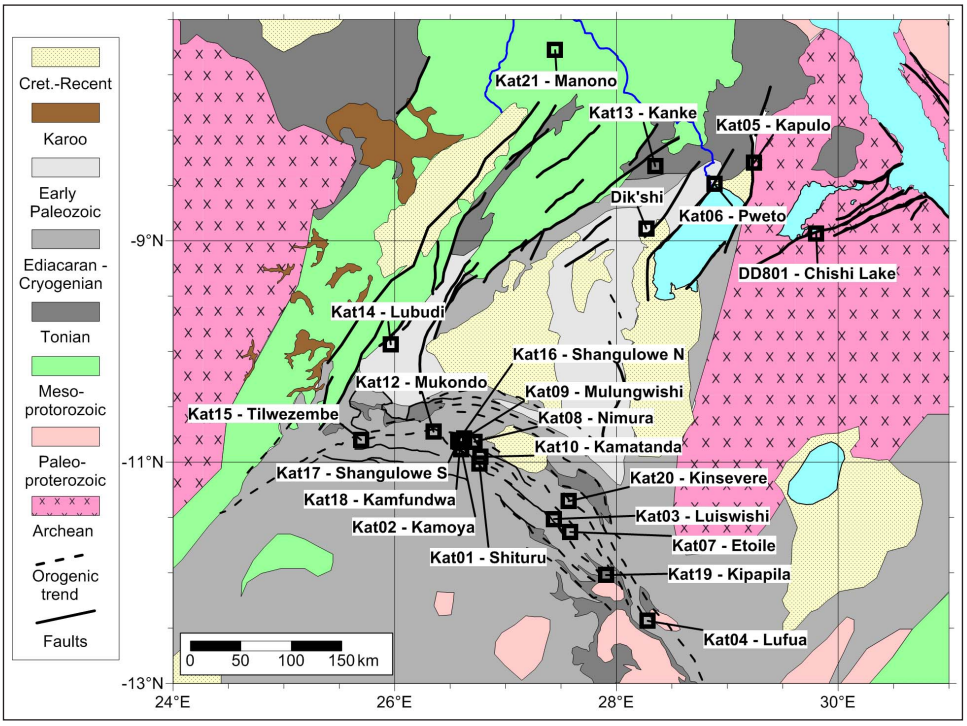

Figure 3. Location of studied sites with their identification on a geological background.

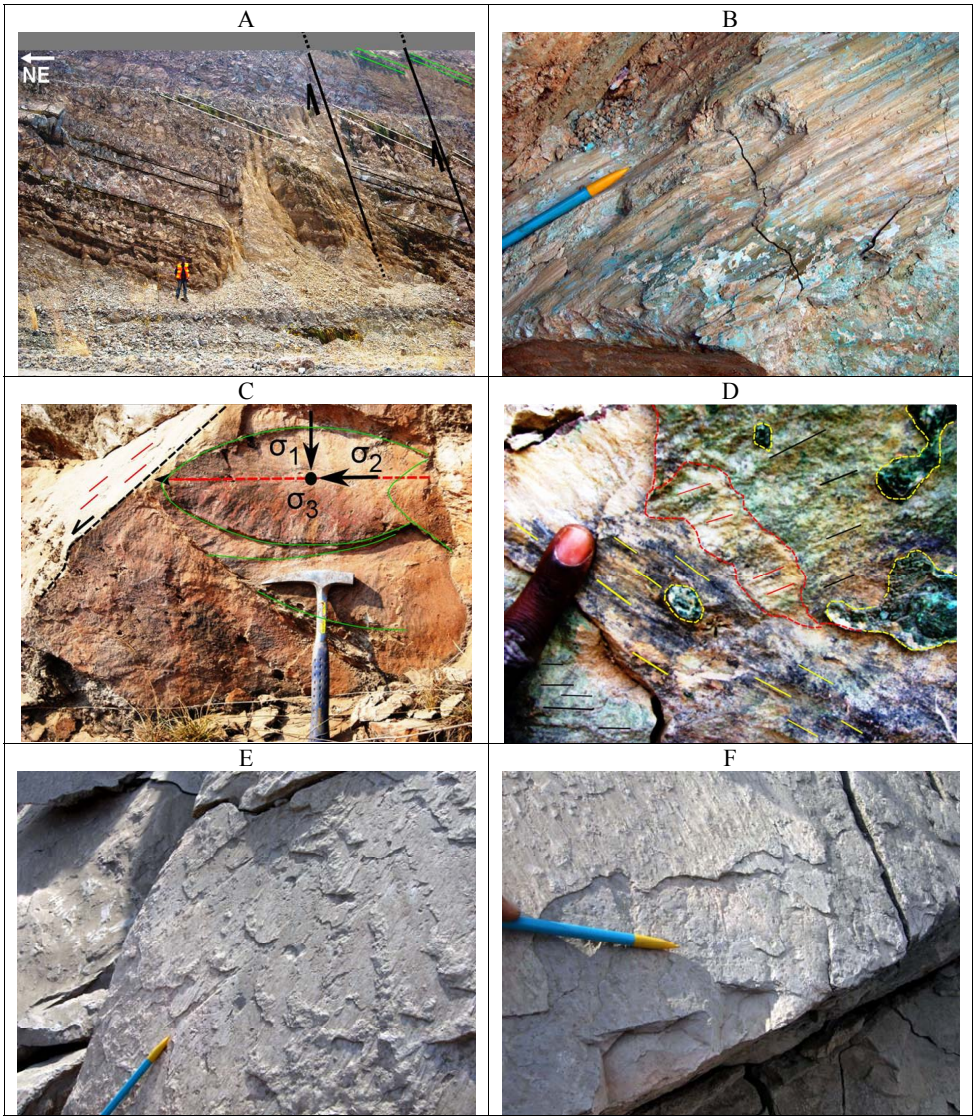

Figure 4. Field examples of fault kinematic indicators. A: Reverse faults affecting the Kundelungu series (Kamfundwa, site 18), B: Example of Cu-dominated mineralized oblique-normal fault with well-expressed slickenline and slip sense indication (Shituru, Kat01), C: Plumose subvertical tension fracture in the Biano series in Pweto, (Kashengeneke hill, Kat 06), D: Superposition of oblique-slip and strike-slip slickenline on a fault plane (Kamatanda, Kat10), E: Oblique-normal reactivation of a bedding plane (Luiswishi, Kat03), F: same as E, superposed on earlier strike-slip slickenlines (parallel to the pen).

and to determine the reduced stress tensor that best explains the observed slip distribution of a population of fault-slip data (e.g. Michael, 1984; Carey-Gailhardis & Mercier, 1987, Marett & Allmendinger, 1990; Sperner et al., 1993; Angelier, 1994; Delvaux & Sperner, 2003, …). As the physical concepts behind these methods are similar, they are all expected to give comparable results (Lacombe, 2012). We used the Win-Tensor program (Delvaux, 2012) which offers great user interaction and capacities for managing integrated database. When compared with other methods on similar data sets, it gives comparable results (e.g. Petit et al., 1996; Delvaux et al., 2010). Win-Tensor is derived from the DOS-based Tensor program (Delvaux & Sperner, 2003). It uses the PBT or Right Dihedra methods for a first approximate estimation of the reduced tress tensor. The latter serves as a starting point in the Rotational Optimization method which performs an iterative testing of a number of solutions using a rotational strategy. For each test, the stress tensor is applied to the fault-slip data by calculating the resolved shear and normal stress on each fault plane. These parameters form the basis of a misfit function (F5 in Win-Tensor) that jointly minimises two terms. The first term exploits the directional part of the resolved shear stress (orientation and sense) for minimizing the misfit angle between the measured slip line and the resolved shear stress on the plane. The second term uses the resolved magnitudes for minimizing the normal stress and maximizing the shear stress on the plane, in order to favour slip. The quality of the results is evaluated using the quality ranking parameter for fault-slip data inversion (Sperner et al., 2003).

For a 2D representation on maps and defining stress trajectories, the results are further converted into 2 parameters: S_{Hmax} and R'. The horizontal principal maximum horizontal stress direction S_{Hmax} is taken as the great axis of the ellipse obtained by the intersection of the stress ellipsoid with the horizontal plane (Lund & Townend, 2007). The stress regime index R' expresses the stress regime numerically, based on the stress ratio R and the nature of the most subvertical stress axes (Delvaux et al., 1997; Delvaux & Sperner, 2003).It ranges from 0 to 1 for extensional regimes, 1 to 2 for strike-slip regimes and 2 to 3 for compressional regimes.

In order to determine the error range for these parameters, the fluctuation of the 4 parameters of the reduced stress tensor is evaluated and used to generate a range of possible stress tensors. These are converted into a series of possible S_{Hmax} and R' values, whose dispersion is expressed by 1σ standard deviations.

3.3. Processing multi-site multi-set data

In several brittle field studies, individual outcrops did not yielded statistically significant data sets to allow reliable stress tensor determination and regional stress tensors are obtained on merged bulk data sets (e.g. Viola et al., 2009, 2011; Kounov et al., 2011). In the Lufilian arc, conversely, most sites yielded datasets sufficiently large to be of statistical significance and often corresponding to several distinct brittle events. The largest sites, as in the Luiswishi Cu-Co deposit (site Kat03), have been subdivide into sub-sites that have been measured independently. Each data set have been processed separately in an initial stage and later grouped to represent the average stress tensors for the entire site (Fig. 5).

The multistage nature of the brittle evolution implies that fault-slip data sets can be heterogeneous in the sense that they cannot be matched by a single stress tensor. Data separation into homogeneous subsets that can be explained by a single stress tensor is then required. We used whenever possible the field-

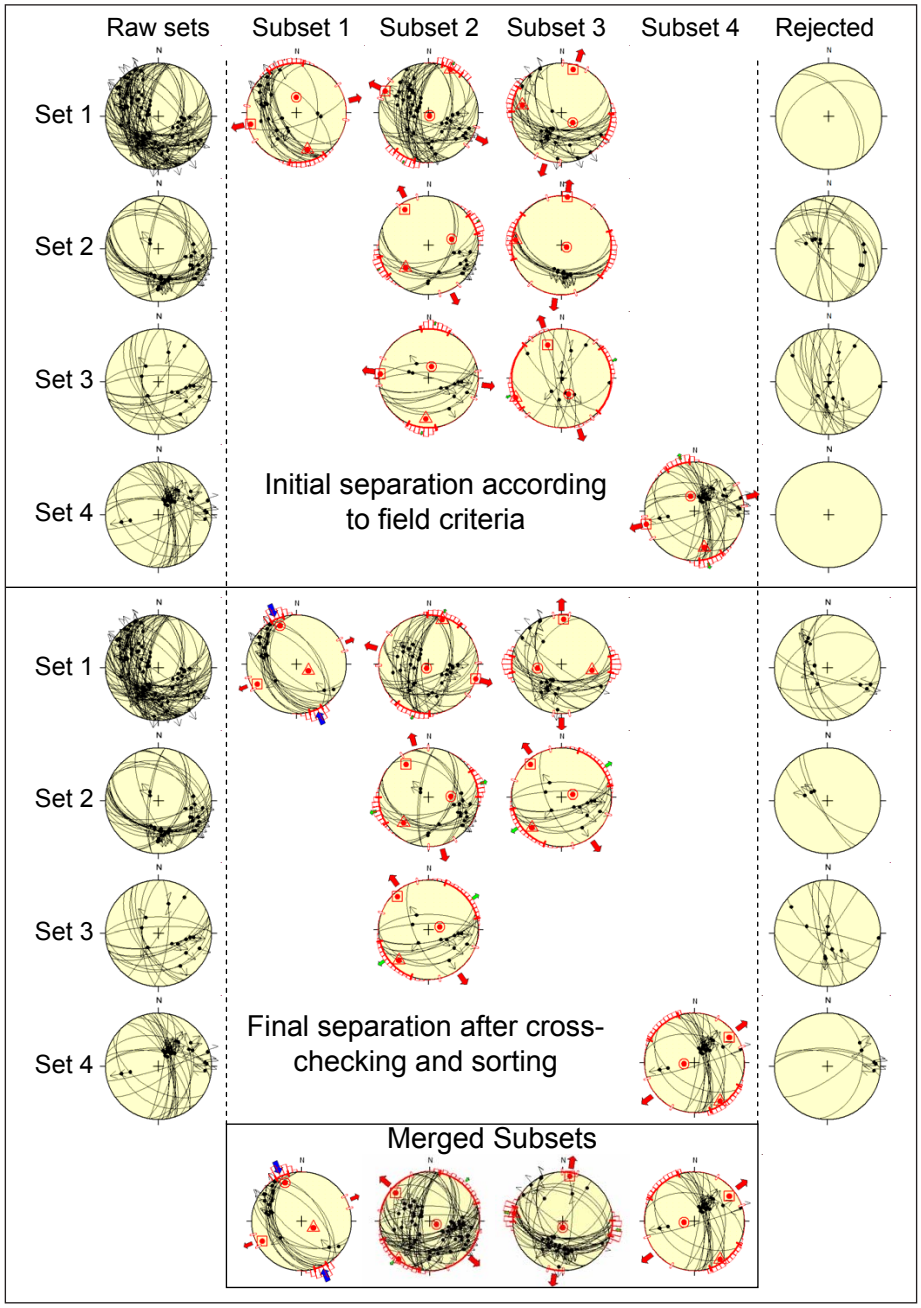

Figure 5. Flow-chart for the processing and separation of fault-slip data from the 3 original data sets measured at different locations of the Luiswhshi deposit (Kat03).

determined subsets as nuclei, in a way similar as proposed by Angelier & Manoussis (1980) but interactively controlled. Each nucleus serves as a basis for an iterative sorting and inversion procedure to filter the original data sets into homogeneous subsets. For each nucleus, a preliminary stress tensor is determined. The preliminary stress tensors are then applied to the total data set and the misfit function determined for each datum. The data are then attributed to the corresponding subset for which the preliminary stress tensor gives the smallest misfit value and those with misfit function F5 higher than a threshold fixed arbitrarily at 30 are eliminated. New stress tensors are determined from the modified subsets. The process is repeated until the system stabilises.

When no subset node could be determined in the field, two procedures can be used. A preliminary tensor is determined on the entire data set with the improved Right Dihedra method and refined using the Rotational Optimization program. The outliers (data with a too high misfit function) are progressively removed (stored in a new subset) and the stress tensor is again optimised. This is repeated until all data have misfit values less than the pre-defined threshold. The rejected data are treated in a similar way and the procedure is repeated until the rejected data are too few or too heterogeneous for extracting a new subset. This procedure is described in Delvaux & Sperner (2003) and works well when one data subset is markedly dominant from the others. If the initial data set contains two or more subsets of equal importance, it will lead to a hybrid subset that contains part of each set (Sperner et al., 2003). In this case, a separation based on the PBT procedure is preferred. In this method, the stress axes are considered equivalent to the average of the individual kinematic p, b and t axes associated to the fault-slip data. When plotted in separate diagrams, one or more of these axes might show a distribution in several clusters. Separation is done for the kinematic axis which shows the best multi-clustering, using these clusters as nuclei. The separated subsets are subsequently treated as in the case of field-determined nuclei.

In Fig. 5, we use the Luiswishi deposit (site Kat03) to illustrate the basic procedure of data sorting and stress tensor determination. It is a megabreccia composed of large fragments of folded structures belonging mainly to the RAT, Mines, Dipeta and Mwashya Subgroups of the Roan Group, considered as megabreccia blocks (Cailteux & Kampunzu, 1995; El Delsouky et al., 2010). These fragments are separated by tectonic breccias formed during and after the main fold-and-thrusting Lufilian deformation. The bedding planes have been intensely reactivated by superposed oblique-slip and normal faulting (Fig. 4 c-d). A total of 185 fault-slip data have been measured in 4 different sub-sites, defining 4 data sets (Fig. 5). For each of the data set, field criteria allow to group the fault-slip data into preliminary subsets or nuclei. Using the cross-cutting relations between individual fault planes and slip striae superposition, 4 subsets

Site	Location					Stage	Data		σ1		σ2		σ3		R	Misfit angle		Shmax		Regime			QR
	Long	Lat	Name	Site	Strati.		N	Nt	pl	az	pl	az	pl	az		Aver.	Max.	Ori.	1σ	R'	1σ	Reg	
Kat01	26,76	-11,01	Shituru	Open mine	Mwashya (R4)	4	35	41	21	139	61	273	19	041	0,70	11,4	31,2	134	5,4	1,30	0,29	SS	B
						4	32	43	10	106	78	252	07	015	0,63	11,2	31,1	105	9,8	1,37	0,45	SS	B
						7	24	25	82	309	08	154	03	064	0,33	10,3	29,3	153	6,8	0,33	0,14	NF	D
Kat02	26,60	-10,88	Kamoya	Open mine	Mines (R2)	2	50	57	01	188	11	278	79	094	0,92	5,5	29,5	6	27,9	2,92	0,16	TF	B
Kat03	27,44	-11,51	Luiswishi	Open mine	RAT (R1) & Mines (R2)	4	19	22	17	337	68	118	13	243	0,21	10,2	31,2	156	7,4	1,79	0,10	SS	C
						5a	51	156	81	125	01	028	08	298	0,29	12,9	35,1	28	29,5	0,29	0,14	NF	B
						5b	38	156	82	180	02	279	09	009	0,91	9,8	38,7	99	8,8	0,91	0,27	NF	B
						7	19	127	74	263	07	146	14	054	0,49	5,9	18,5	142	24,7	0,49	0,21	NF	E
Kat04	28,28	-12,43	Lufua	Open mine	Mwashya (R4)	3	14	113	15	069	45	175	41	326	0,14	6,8	19,3	68	7,6	1,86	0,12	TS	E
						4	34	113	54	356	21	120	27	221	0,80	8,4	33,1	134	17,3	0,80	0,19	NF	C
						5	13	113	75	211	09	087	12	355	0,61	6,8	17,5	84	5,2	0,61	0,15	NF	E
						6	14	113	03	113	60	208	30	022	0,36	7,6	18,8	112	7,6	1,64	0,23	SS	E
						8	19	113	72	010	14	227	10	134	0,38	6,8	22,1	40	13,4	0,38	0,16	NF	D
Kat05	29,24	-8,30	Kapulo	Road section	Coarse pink granite	3	28	30	01	252	77	348	13	162	0,50	0,1	2,2	72	13,9	1,50	0,25	SS	D
						7	23	23	75	339	13	133	06	224	0,28	4,9	25,4	138	24,9	0,28	0,13	NF	C
						8	36	36	65	193	15	067	19	331	0,50	3,3	28,1	55	27,6	0,50	0,17	NF	C
Kat06	29,88	-8,49	Pweto (Kashen-geneke)	Road section	Plateaux / Biano (Ku3)	3	30	101	16	050	68	185	15	316	0,83	6,7	27,5	46	7,4	1,17	0,09	SS	C
						6a	42	101	02	144	13	053	77	246	0,02	5,9	23,7	144	8,1	2,02	0,20	TF	B
						6b	29	101	13	305	23	042	63	188	0,13	6,9	22,9	124	13,6	2,13	0,16	TF	D
Kat07	27,58	-11,63	Etoile	Open mine	Dipeta (R3) Mines (R2)	1	31	77	32	004	05	271	57	174	0,21	11,6	31,0	5	12,6	2,21	0,12	TF	C
						2	31	77	34	213	10	116	55	011	0,38	5,9	17,7	41	28,9	2,38	0,16	TF	B
						5	29	51	74	112	07	227	15	318	0,12	4,9	18,2	66	35,1	0,12	0,08	NF	C
						6	13	51	02	131	17	040	73	227	0,35	4,1	9,7	131	12,3	2,35	0,16	TF	D
						7	14	77	77	319	13	156	04	065	0,21	8,0	20,3	153	17,0	0,21	0,10	NF	D
Kat08	26,72	-10,82	Nimura	Open mine	Mines (R2) Mwashya (R4)	1	24	43	21	356	02	086	69	180	0,47	7,1	24,4	175	28,0	2,47	0,21	TF	C
						3	9	43	05	034	81	158	07	304	0,69	7,2	14,1	34	6,6	1,31	0,21	SS	D
Kat09	26,63	-10,79	Mulungwishi	Open mine	Mwashya (R4) Nguba	1	12	49	30	130	05	038	59	299	0,55	2,4	11,1	137	38,4	2,55	0,28	TF	D
						3	13	49	57	349	12	239	30	142	0,94	0,7	3,6	51	16,5	0,94	0,16	NF	D
						5	18	49	76	144	09	16	11	284	0,50	3,8	9,5	12	23,7	0,50	0,20	NF	C
Kat10	26,77	-10,95	Kamatanda	Open mine	Mines (R2)	1	25	72	37	357	01	266	54	175	0,57	4,4	23,3	3	48,1	2,57	0,37	UF	B
						2	8	72	03	320	01	229	86	118	0,96	4,9	8,7	142	43,0	2,96	0,07	TF	D
						3	14	72	25	061	14	324	61	207	0,09	8,2	24,5	62	4,5	2,09	0,09	TF	C
						4	16	72	38	159	44	299	21	051	0,48	8,5	18,7	149	9,5	1,52	0,19	UF	D
Kat12	26,35	-10,72	Mukondo	Open mine	Mines (R2)	3	10	61	26	265	58	048	16	167	0,09	3,0	13,8	84	5,3	1,9	0,1	SS	E
						4	26	61	33	348	50	209	21	092	0,21	4,6	16,3	172	11,0	1,8	0,2	UF	B
						5	13	61	52	359	37	173	03	265	0,66	3,7	9,6	176	7,5	0,7	0,2	NS	D
						7	10	61	67	335	14	100	18	195	0,42	2,7	9,4	112	19,2	0,4	0,2	NF	D
Kat13	28, 35	-8,33	Kanke	Fault-	Kundelungu	7	35	35	80	52	4	165	9	256	0,23	6,9	29,0	168	27,9	0,2	0,2	NF	B
Kat14	25,96	-9,94	Lubudi	Open mine	Kundelungu (Ku)	1	14	89	15	219	3	128	75	29	0,77	5,1	11,6	42	30,7	2,8	0,3	TF	C
						2	32	89	17	35	71	239	7	127	0,52	7,0	25,5	36	10,9	1,5	0,2	SS	C
						3	19	89	8	68	81	225	4	338	0,5	2,1	11,4	68	16,2	1,5	0,6	SS	D
						8	20	89	70	358	10	240	18	146	0,37	5,8	37,4	50	14,9	0,4	0,2	NF	D
Kat15	25,70	-10,80	Tilwezembe	Open mine	Mwashya (R4) & Gr.cong. (Ku)	1	5	55	13	120	34	219	54	12	0,71	5,4	7,2	111	18,7	2,7	0,2	TF	E
						3	22	55	6	32	78	270	10	122	0,41	6,8	23,1	32	4,5	1,6	0,2	SS	B
						5	13	55	74	25	13	175	8	267	0,53	4,8	11,6	178	6,7	0,5	0,2	NF	D
						7	11	55	57	121	31	278	10	15	0,22	8,8	19,5	113	15,2	0,2	0,1	NF	D
Kat16	26,57	-10,81	Shangulowe North	Artisanal mine	Kundelungu (Ku) Sedimentary breccia	1	70	188	7	144	29	50	60	247	0,30	9,5	26,8	145	11,8	2,3	0,2	TF	B
						3	30	188	31	251	59	61	5	157	0,82	2,5	22,3	69	9,1	1,2	0,2	SS	D
						5	35	188	69	98	2	2	20	271	0,79	3,9	22,0	1	17,4	0,8	0,2	NF	D
						6	25	188	39	295	50	101	8	199	0,63	7,5	31,1	111	10,0	1,4	0,2	SS	E
Kat17	26,57	-10,81	Shangulowe South	Artisanal mine	Idem	4	15	73	28	302	60	143	9	37	0,64	4,0	14,0	125	4,2	1,4	0,45	SS	E
						7	31	73	80	76	6	307	7	216	0,24	7,5	31,4	123	17,3	0,2	0,12	NF	C
Kat18	26,59	-10,82	Kamfundwa	Open mine	Mines (R2)	1	15	53	8	354	6	262	80	140	0,33	5,4	22,7	174	8,1	2,3	0,2	TF	D
						2a	16	53	0	54	7	324	83	140	0,9	2,4	11,0	54	20,4	2,9	0,2	TF	B
						2b	8	53	19	294	1	204	71	108	0,8	3,4	7,6	117	39,5	2,8	0,3	TF	D
						2c	6	53	12	139	43	239	45	36	0,7	2,4	5,0	132	13,6	2,7	0,2	TS	E
Kat19	27,91	-12,02	Kipapila	Open mine	Mines (R2)	1	28	125	22	149	13	53	64	295	0,90	4,7	30,7	10	37,1	2,9	0,3	TF	D
						3	16	125	29	206	60	42	7	300	0,83	4,0	13,5	29	9,9	1,2	0,2	SS	E
						7	44	125	76	274	8	149	11	58	0,11	10,7	31,7	134	34,6	0,1	0,1	NF	C
						8	12	96	66	45	24	243	7	150	0,99	5,0	13,3	60	11,1	1	0,2	NF	E
Kat20	27,57	-11,35	Kinsevere	Open mine	Mines (R2)	2	92	408	01	035	17	125	73	303	0,40	8,7	35,8	035	13,8	2,40	0,21	TF	B
						3	51	239	01	255	52	347	38	164	0,19	11,9	33,6	075	5,3	1,81	0,14	SS	E
						6	66	239	19	114	59	351	24	213	0,01	6,6	36,8	114	2,6	1,99	0,03	SS	D
Kat21	27,45	-7,28	Manono Hospital	Old & artisanal mine	Kibaran micaschist & pegmatite	1	37	275	18	200	14	296	66	58	0,6	12,2	33,7	12	16,6	2,6	0,1	TF	D
						3	74	275	3	68	59	163	31	336	0,2	13,2	34,0	68	7,1	1,8	0,2	SS	D
						6	39	275	27	319	30	211	47	83	0,1	6,6	21,1	141	7,1	2,1	0,1	UF	E
						8	78	275	74	257	14	44	8	137	0,6	12,6	30,2	48	13,2	0,6	0,2	NF	D
DD803	29,80	-8,94	Chishi Lake	Kalate	Mbale	3	32	22	03	055	77	313	13	145	0,15	10,7	38,0	055	9,9	1,85	0,41	SS	E
Dik'shi	28,27	-8,89	Dikulushi	Open pit	Kundelungu (Ku1-2)	3	14	42	21	061	62	285	17	158	0,08	7,0	23,1	062	7,9	1,92	0,12	SS	C
						6	13	42	03	162	11	252	79	053	0,48	13,3	25,8	162	7,9	2,48	0,20	TF	C
						8	6	42	65	360	19	222	16	126	0,64	16,8	36,6	033	20,7	0,64	0,28	NF	E

Table 1. Stress tensor results with brittle stages displayed chronologically for each site. N: number of data used in the subset; Nt: total number of measured data (before separation); σ1, σ2, σ3: stress axes; pl: plunge, az: azimuth; R: stress ratio; S_{Hmax}: horizontal maximum compressional axes with 1σ standard deviation; R': stress regime index with, 1σ: standard deviation for R', Reg: stress regime; Qual QR: Quality factor (A: excellent, B: good, C: medium, D: bad). Average and maximum misfit angle using function F5.

are defined and correlated between the different sub-sites. Those are treated in a first step to propose preliminary stress tensors with a relative chronology in function of the field classification (Fig. 5, upper part). At this stage, no separation has been done and the some subsets can still be heterogenous. Separation is done using the interactive procedure described above in order to obtain homogeneous subsets (Fig. 5, lower part). Finally, equivalent subsets from the different sub-sites are combined in larger subsets that are statistically more significant, one for each represented stress stage (Fig. 5, bottom).

A similar procedure is applied for all large measurement sites, adapted in function of the local situation.

4. Stress tensor results

After processing all sites, 70 stress tensors have been obtained, representing a total of 1889 fault-slip data for the 22 investigated sites (86 data in average per site and 27 per tensor). This significant data set allows to identify 8 different stress stages and to determine their relative chronology (Fig. 6). A maximum of 5 successive stages have been obtained from the same site. The correlation proposed is based on an integrated evaluation of the results, their spatial and temporal relations, fault cross-cutting relationships and striae superposition and overall consistency in terms of stress field evolution. The spatial subdivision of the data into 3 different sub-regions (Lufilian arc, Kundelungu foreland, Kibaran belt) and the integration of the results from the Ubende belt (Delvaux et al., 2012) allow to differentiate regional brittle events (that affect all the studied region in an homogenous way) from local ones (that affect only the Lufilian arc).

The main information derived from the 21 sites is summarised in Fig. 6, detailed in map view for the successive stage in Fig. 7 and reported in table 1. The fault-slip data and stress results for each stage have been grouped together and displayed as rose diagrams and histograms (Fig. 8). For each stage, the average stress tensor has been determined without additional separation (Fig. 9, Table 3).

5. Brittle tectonic stages and paleostress evolution

We consider that each of the 8 stress stages identified represents a brittle deformation event related to the geodynamic history of the Lufilian orogen (near-field stresses) or at a plate scale (far-field stresses). These brittle events are interpreted in function of possible geodynamic causes and compared with brittle tectonic evolution determined in other sectors of the Subequatorial Africa from the time of the Lufilian paroxysm, up to the present-day

Site	Data	S_{Hmax}		Reference		Unfolding	
Ref	N	Orient.	1σ	Structural trend	Deviation S_{Hmax} - Trend	Deviation Trend - N140°E	Unfolded S_{Hmax}
Kat15	5	111	19	70	41	70	1
Kat16	70	145	12	100	45	40	5
Kat18	15	174	8	100	74	40	34
Kat09	12	137	38	100	37	40	-3
Kat08	24	175	28	110	65	30	25
Kat10	25	183	48	130	53	10	13
Kat 07	31	185	13	140	45	0	5
Kat19	28	190	37	155	35	-15	-5
Averages		163			51		11
Standard deviations		28			14		14

Table 2. Unfolding of the S_{Hmax} orientations of the stress tensors obtained for the first stage in the Lufilian arc, with a reference pre-folding trend of N140°E.

(Viola et al., 2008; 2012; Delvaux & Barth, 2010; Delvaux et al., 2012).

Stage 1: Early N-S compression

The first brittle stage recorded affects the entire Lufilian arc, its lateral contact with the Kibaran belt (Lubudi, Kat 14) and also the Kibaran belt itself at Manono (Kat21) (Fig. 7a). It is related to a general N-S tectonic compression and is expressed by barren fractures. The associated brittle structures are trending dominantly E-W and are moderately to steeply dipping. The rake (seismological notation equivalent to the pitch angle with indication for the slip sense) show dominantly dip-slip reverse faulting (+80-100°), consistently with the stress regime index R' which averages 2.5 (Fig. 8, Table 3).

The associated S_{Hmax} directions are diversely oriented in a fan shape, spatially related to the curved shape of the belt. Within the Lufilian arc itself, the S_{Hmax} directions tend to remain at a high angle to the local trend of the belt (51 ± 14° in average, Table 2), with a systematic clockwise relation. In the Kibaran belt, the Manono site shows a nearly N-S S_{Hmax} orientation which is markedly different from the ones in the eastern part of the Lufilian arc but relatively similar to the ones in the central and south-eastern parts of the arc. This suggests that the north-western part of the Lufilian belt could have been bent in an orocline after the development of the compressional brittle structures, causing the anticlockwise rotation of the recorded paleostress directions, with the south-eastern part of the orogen remaining in its pre-brittle orientation.

To test this hypothesis, we unfolded the stress tensors recorded in the Lufilian arc, taking the average trend of its south-eastern part (N140°E) as a reference (Table 2). We do not consider this trend as the original trend of the belt but the as general trend when the first stage of brittle faulting was recorded. This trend was probably inherited from earlier orogenic deformation witch could have been in a more ductile way. We rotated the stress results in the Lufilian arc clockwise around a vertical axis according to the deviation between the local and the reference trends, in order to bring the local trend of the belt towards parallelism with the NW-SE orientation of the belt on its south-eastern side. After unfolding, the 8 restored stress data in the Lufilian arc (unfolded S_{Hmax} in Table 2 and labelled stage 1r in Fig. 6) display more constant S_{Hmax} orientations. The standard deviation for S_{Hmax} of these 8 sites is lower (14°) after the unfolding than before (28°; Table 2), as illustrated by the S_{Hmax} rose diagrams (Fig. 8, stage 1). This validates the folding test and suggests that the bending of the Lufilian arc occurred after the first stage of compressional brittle faulting.

Stage 2: Constriction in the central part of the arc

Brittle deformation in the central part of the Lufilian arc (e.g. Kambove area: Kat 02 and Kat 18) is characterized by a dominance of 40-60° dipping slip planes that show reverse dip-slip striae regardless of their orientation (Figs 7b, 8). They often accompany injected tectonic breccias with intense block rotations in a context of vertical extrusion (Jackson et al., 2003). Most of the related stress tensors show axial compression (constriction), with most R' values above 2.8. The S_{Hmax} orientations display a large variety of orientation as would be expected because with axial compression, the σ1 and σ2 stress axes which are both sub horizontal have relatively comparable magnitude and are nearly equivalent. This type of deformation is spatially related to the hinge zone of the Lufilian arc where orogenic bending has been the most intense, and has not been recorded outside the fold-and-thrust belt domain. It is therefore attributed to constrictional deformation caused by the oroclinal bending of the Lufilian arc.

Stage 3: Regional NE-SW transpression

After oroclinal bending, the Lufilian arc underwent important NE-SW transpressional deformations that are recorded in the Kundelungu foreland and in the Kibaran belt (stage 3). They give strike-slip stress tensors with an average NE-SW S_{Hmax} direction (N58°E) and a transpressional component (average R' = 1.6, Table 3). It is the best expressed brittle stage, recorded at 15 different sites by 376 faults/fractures and 238 slip lines (Fig. 7c, Table 3). It is correlated with the NE-SW compression observed in the Ubende belt, on the other side of the Bangweulu block (Delvaux et al., 2012).

The fractures are generally oriented NE-SW, are dominantly high-angle with strikes-slip striae and right-lateral movement as indicated by the high rake angle (close to +/- 180°; Fig. 8). It generated dextral strike-slip faulting in the Kundelungu foreland along the Bangweulu block and at the margin of the Kibaran belt and brecciated transverses fault zones in the central and western parts (Fig. 7c) The N-S trending eastern part of the arc has not been studied in sufficient detail, but we relate the Monwezi-type arc-parallel left-lateral strike-slip faulting of François (1984) and Kampunzu & Cailteux (1999) to this stage.

Stage	Data	Tensors	σ1		σ2		σ3		R	S_H		Regime		Misfit angle	
	N		pl	az	pl	az	pl	az		Max	1σ	R'	1σ	Aver.	Max.
1	261	10								153	25	2,54	0,22	7	22
		average	4	347	10	79	79	237	0,78	165	27	2,78	0,24	30	179
2	242	8								70	27	2,58	0,18	5	16
		average	1	25	8	116	82	291	0,51	25	16	2,51	0,20	18	125
3	376	15								58	9	1,57	0,21	6	20
		average	1	236	87	131	3	327	0,3	56	9,4	1,70	0,23	25	180
4	177	7								139	9	1,42	0,26	8	25
		average	4	312	84	90	4	222	0,47	132	7	1,53	0,35	38	147
5 NW	79	4								2	14	0,62	0,19	4	13
		average	81	165	9	3	3	273	0,68	3	5,8	0,68	0,20	11	82
5 SE	131	4								69	20	0,48	0,16	9	27
		average	78	131	6	249	11	340	0,21	74	46	0,21	0,09	20	133
6	241	8								130	9	2,01	0,15	7	24
		average	4	322	39	228	50	56	0	142	10	2,00	0,09	15	174
7	211	9								137	21	0,28	0,14	7	24
		average	82	337	8	155	0	245	0,16	155	17	0,16	0,10	15	123
8	171	6								48	17	0,58	0,20	8	28
		average	87	9	2	230	2	140	0,55	50	10	0,55	0,18	19	107
Total	1889														

Table 3. Average results for the 8 brittle stages. Upper line: average S_{Hmax}, R' and misfit angle for the stress tensor result of the related sites. Lower line: average stress obtained by the stress inversion of all the fault-slip data attributed the each stage (stereograms displayed in Fig. 9).

Stage 4: Transtension after σ1 – σ3 permutation

Strike-slip deformations attributed to brittle stage 4 are recorded only in the fold-and-thrust belt sector (Fig. 7d, displaying S_{hmin} directions). It is expressed by high-angle normal faults, trending NE and with oblique-slip striae (rake angles between 110 and -120°; Fig. 8). Some of them reactivate bedding planes as in Luiswishi (Fig. 4f). The stress tensors display a transtensional component (R' = 1.4) and differ from those of stage 3 by a permutation of the horizontal stress axes σ1 and σ3, bringing S_{hmin} in parallelism to the S_{Hmax} direction of the preceding stage (Fig. 7c, displaying S_{Hmax} directions). This stage caused important mineral remobilisation as for example in the Shituru deposit (Fig. 4a). It marks the onset of late orogenic extension in the Lufilian arc.

Stage 5: Arc-parallel extension

Late-orogenic normal faulting is well represented throughout the entire Lufilian arc (Fig. 7e, displaying S_{hmin} directions).

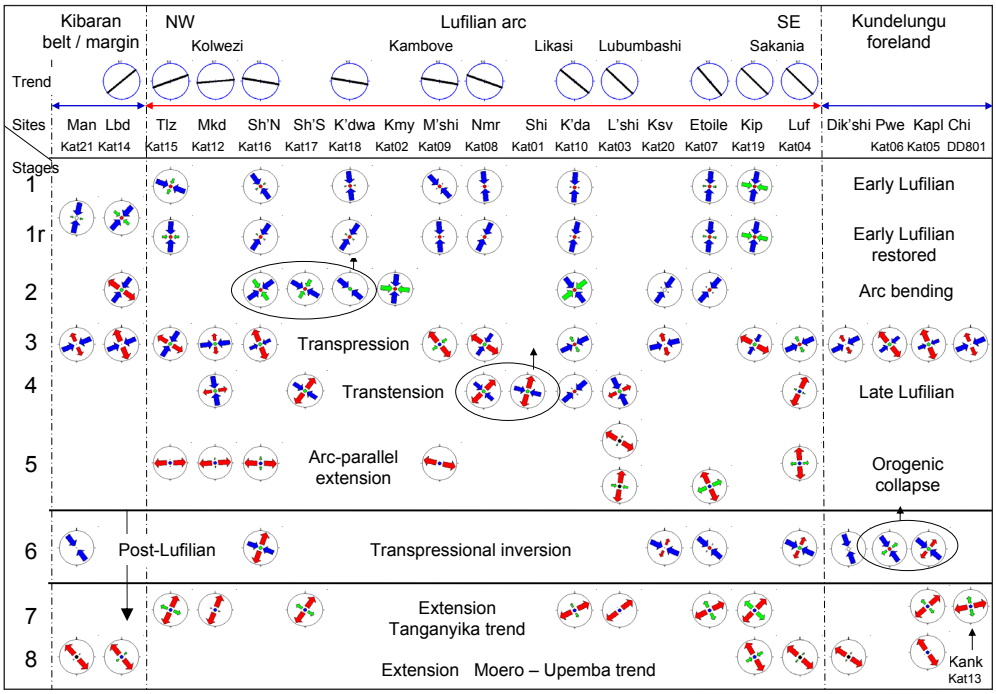

Figure 6. Synthetic table presenting the stress results for all sites, assembled into stress stages. Stress symbols show the horizontal stress axes (S_{Hmax} and S_{hmin}). Their length and colour are function of the stress ratio R and stress regime: red outward arrows for σ_3, green arrows for σ_2 (outward for transtensional and inward for tanspressional), blue inward arrows for σ_1 axis. The central solid circle symbolises the stress regime: red for extensional, green for strike-slip and blue for compressional.

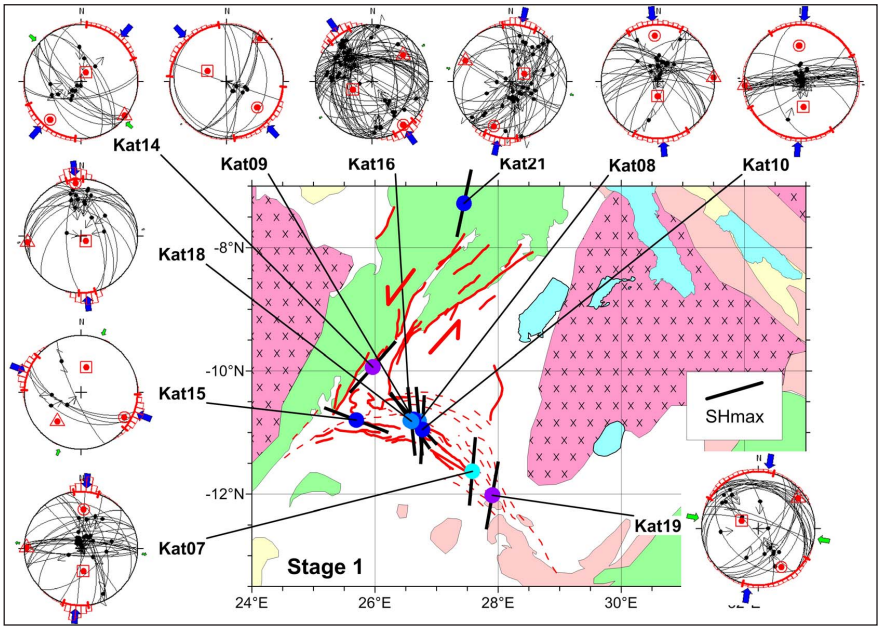

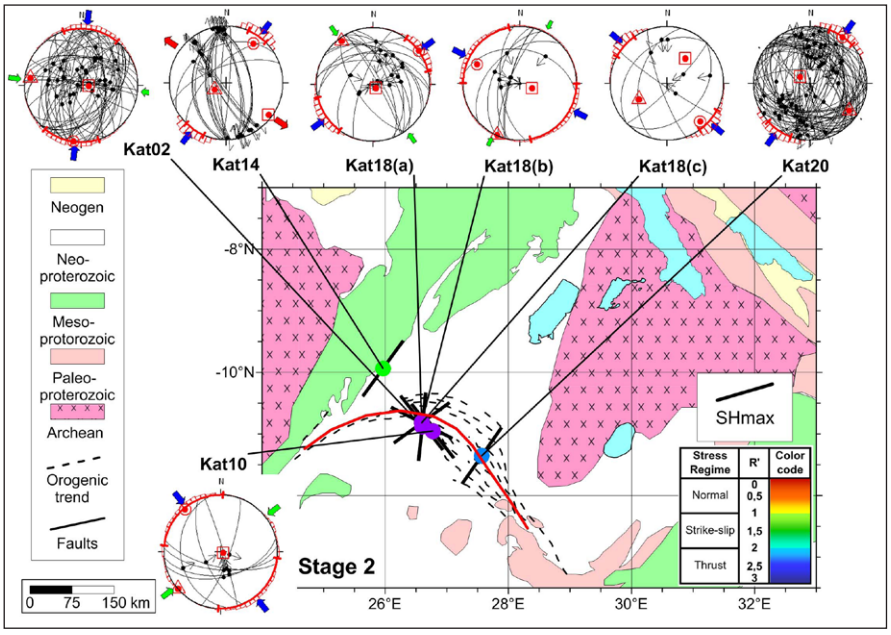

Figures 7a-e. Stress maps for the 8 brittle stages, with the fault system active during the considered stage, S_{Hmax}/S_{hmin} orientations as black/red bars and filled circle coloured in function of the stress regime index R'. Detailed stereograms with the fault-slip data, stress axes and statistical variablilty of the S_{Hmax} orientation (in red, on the external circle). Fault-slip data are displayed as great circle for planes and slip line with slip sense.

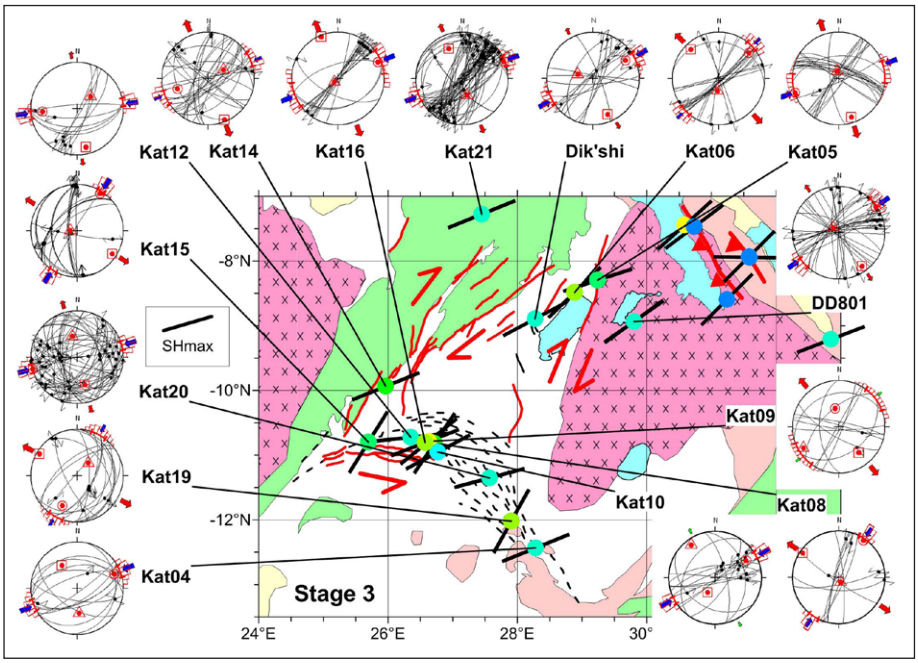
Kat12
Kat14
Kat16
Kat21
Dik'shi
Kat06
Kat05
Kat15
DD801
SHmax
Kat20
Kat09
Kat19
Kat10
Kat08
Kat04
-8°N
-10°N
-12°N
Stage 3
24°E
26°E
28°E
30°

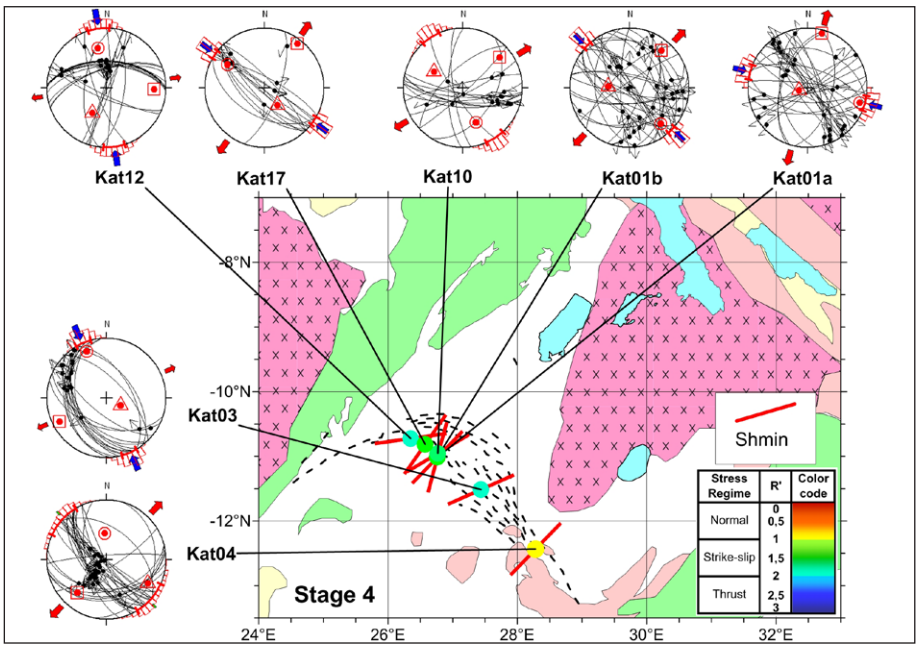
Kat12
Kat17
Kat10
Kat01b
Kat01a
-8°N
-10°N
-12°N
Kat03
Kat04
Shmin
Stress Regime
R'
Color code
Normal
Strike-slip
Thrust
0
0,5
1
1,5
2
2,5
3
Stage 4
24°E
26°E
28°E
30°E
32°E

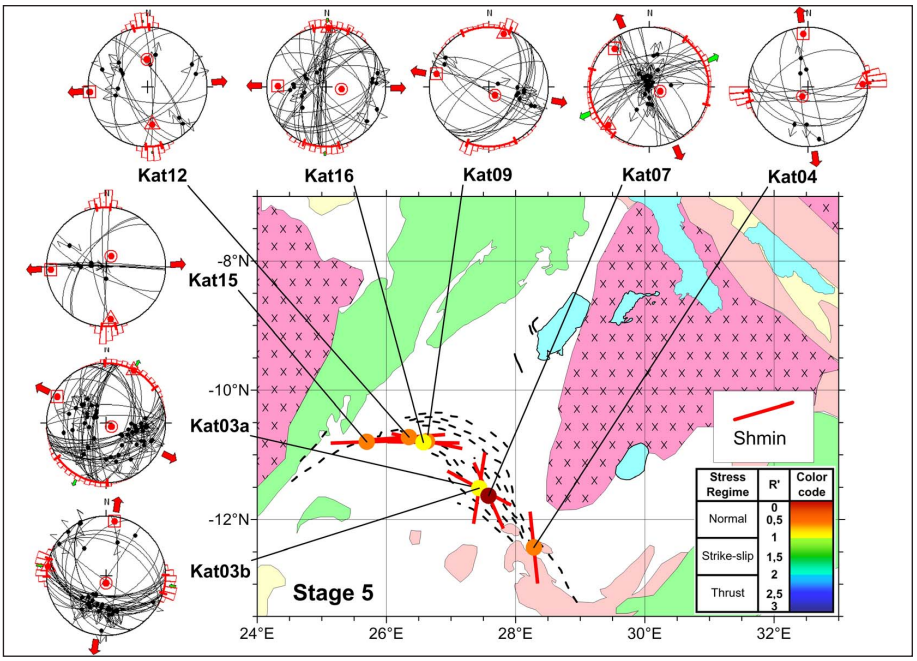
Kat12
Kat16
Kat09
Kat07
Kat04
Kat15
-8°N
-10°N
-12°N
Kat03a
Kat03b
Shmin
Stress Regime
R'
Color code
Normal
Strike-slip
Thrust
0
0,5
1
1,5
2
2,5
3
Stage 5
24°E
26°E
28°E
30°E
32°E

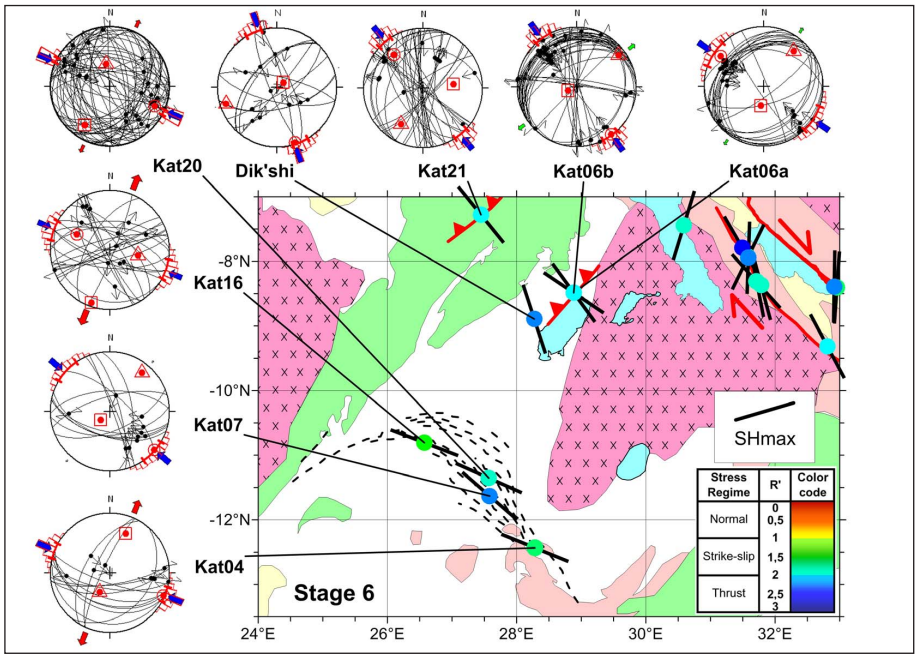
Kat20
Dik'shi
Kat21
Kat06b
Kat06a
Kat16
Kat07
Kat04
-8°N
-10°N
-12°N
24°E
26°E
28°E
30°E
32°E
SHmax
Stage 6
Stress Regime
R'
Color code
Normal
Strike-slip
Thrust
0
0,5
1
1,5
2
2,5
3

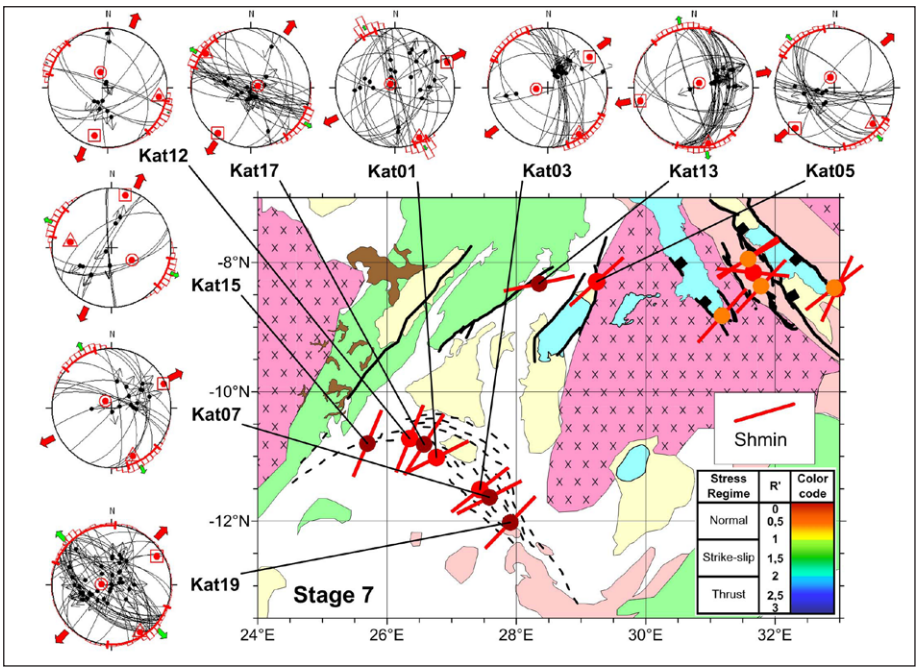
Kat12
Kat17
Kat01
Kat03
Kat13
Kat05
Kat15
Kat07
Kat19
-8°N
-10°N
-12°N
24°E
26°E
28°E
30°E
32°E
Shmin
Stage 7
Stress Regime
R'
Color code
Normal
Strike-slip
Thrust
0
0,5
1
1,5
2
2,5
3

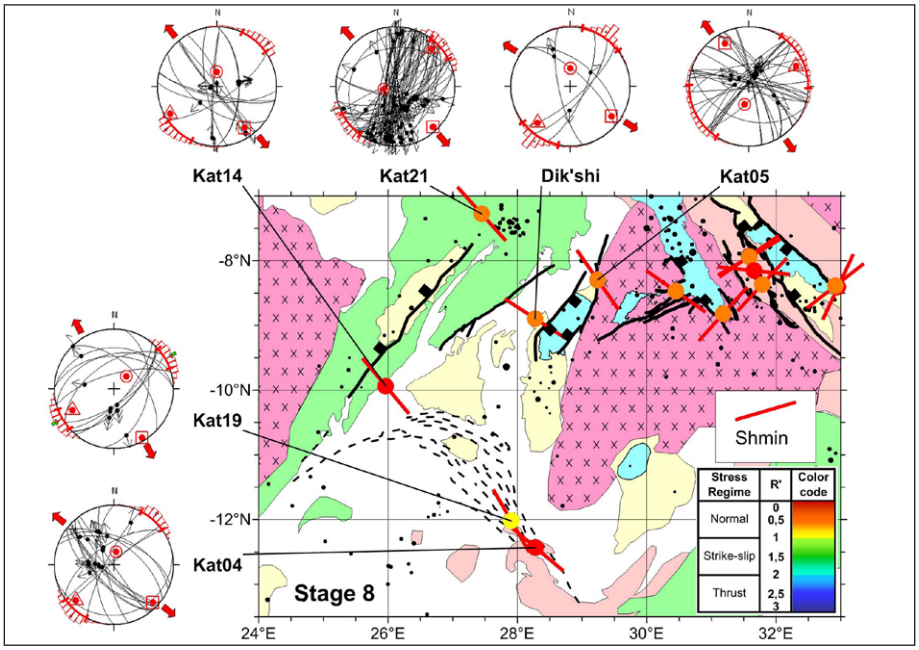
Kat14
Kat21
Dik'shi
Kat05
Kat19
Kat04
-8°N
-10°N
-12°N
24°E
26°E
28°E
30°E
32°E
Shmin
Stage 8
Stress Regime
R'
Color code
Normal
Strike-slip
Thrust
0
0,5
1
1,5
2
2,5
3

It reactivated among others steeply inclined bedding planes (as in Luiswishi, Fig. 4e-f). The average stress regime is of pure normal faulting (R' = 0.5-0.6, and the direction of horizontal extension (S_{hmin}) lies in general parallelism to the trend of the Lufilian arc, following its arcuate shape (N92°E in the NS part and N69°E in the SE part). Extension is dominated by dip-slip normal faulting (rake angle: - 70 to -80°) with fault plane trending generally N-S in the NW part and E-W in the SE part of the belt (Fig. 8). In the SE part, many fault planes are less steeply inclined than the usual 60° as expected for normal faults, reflecting the frequent reactivation of the folded bedding planes.

Stage 6: Regional NW-SE transpressional inversion

After the extensive normal faulting with mineral remobilization that characterises the late-orogenic arc-parallel extension of stage 5, the Lufilian arc and Kundelungu foreland have been affected by reverse to oblique-slip faulting (stage 6). Correlated with the second brittle stage in the Ubende belt (Delvaux et al., 2012), they represent a regional phase of brittle transpressional inversion (Fig. 7f). At Lufua (Kat 04) and Shangulowe North (Kat 16) in the arc as well as the Kashengeneke Mountain (Kat 06) in the foreland, compressional structures have been observed in the upper series of the Kundelungu Group (Biano Sub-group), indicating a Post-Lufilian age. The horizontal compression remains constant in a NW-SE to WNW-ESE direction across the entire Lufilian arc and its foreland, without an apparent influence from the local structures. The average stress regime is strike-slip to transpressional (R' = 2.0) and the rake angles (Fig.

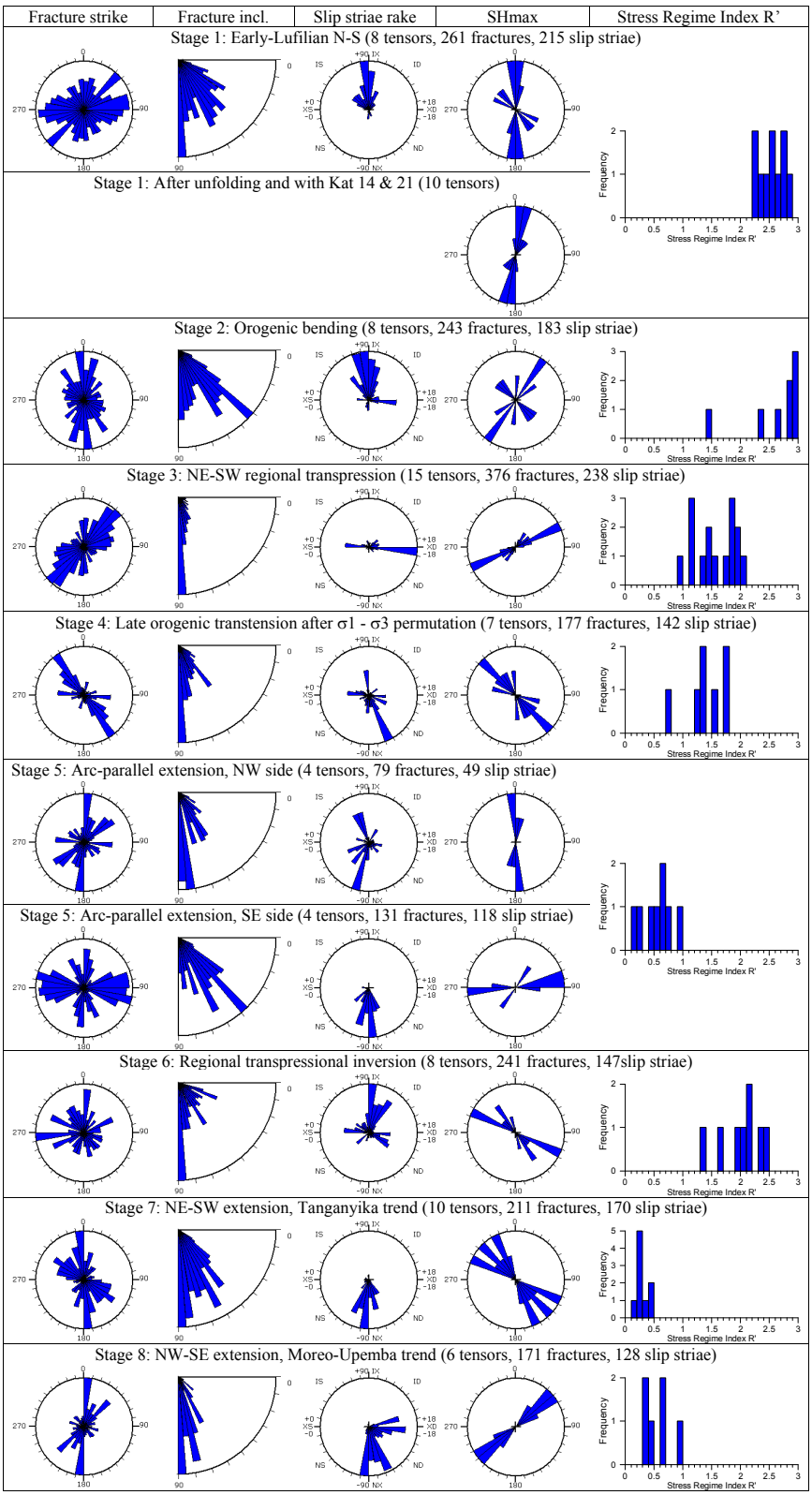

Figure 8. Synthetic Rose diagrams and histograms for the 8 brittle stages.

8) show maxima close to 0 (left-lateral), +/- 180 (right-lateral) and +90° (reverse faulting). This stage did not caused mineral remobilisations.

Stages 7 & 8 : rift-related extension

The last two brittle stages (Figs 7g-h, displaying S_{hmin} directions) are related to the extensional context that prevailed in East Africa after the transpressional inversion. They caused additional normal faulting in the mineral deposits of the Lufilian arc along large dip-slip faults, with locally important mineral remobilizations. We identified a first well-represented normal faulting stage with horizontal extension in a NNE-SSW to NE-SW direction, at a high angle to the Tanganyika rift (stage 7 - Tanganyika rift trend, Fig. 7g). The average stress regime (R' = 0.3) indicates the presence of a radial component of extension. A second normal faulting stage terminates the long brittle tectonic history, with a slight transpressional component (R' = 0.6) and a horizontal extension at the high angle of the NE-trending Moero and Upemba rift basins (stage 8 - Moero-Upemba Rift Trend, Fig. 7h). It is also observed in the Lufilian arc at a mine site of Kipapila (Kat 19) closed to the Domes region. At Kanke (Kat 13), near the Kapulo Cu-deposit along the Moero fault system, Cu-mineralizations (chrysocolla and azurite) are observed in tension fractures and could be related to syn-rift remobilizations. The rakes show that, in addition to a dominant dip-slip faulting (angles close to -90°), minor dextral strike-slip faulting also occurred (angles close to +/- 180°).

The time relation between these two extensional stages is not clear from field relationships, but we consider stage 8 as the youngest because it is related to the development of the inscipient SW-branch of the EARS that is considered as a new rift branch (Scholz et al., 1976; Sebagenzi et al., 2002; Kinabo et al., 2007) and because it corresponds to the present-day stress field determined from earthquake focal mechanisms (Delvaux & Barth, 2010).

7. Tectonic interpretation

The succession of brittle tectonic stages and their stress field characteristics provide additional constraints to refine the knowledge on the tectonic development of the Lufilian arc. Some of our brittle stages can be related to known deformation stages evidenced on the basis of regional mapping and detailed mining exploration (e.g. François, 1987; Kampunzu & Cailteux, 1999). They have been integrated in a larger, regional context using brittle data from area surrounding the Lufilian arc. Other brittle stages correspond to deformation stages not yet or still poorly described, illustrating the late to post-orogenic extension in the Lufilian arc and the more recent rifting evolution.

Onset of brittle realm

The first documented episode of brittle deformation affect already folded structures. Therefore, the earliest brittle tectonic stage may represent only part of the total tectonic evolution of the Lufilian belt. It is not clear weather the fold-and-thrust belt had once a ductile or semi-ductile evolution or if deformation simply started by folding, with faulting appearing in a later stage. We approximate that the system enter the brittle realm at a time close to the orogenic paroxysm, estimated at ~ 550 Ma (Porada & Behorst, 2000; John et al., 2004).

Lufilian first brittle compression

The first brittle stage in the Lufilian recorded a compressional stress regime. It can be related to the D1 - Kolwezian deformation stage of François (1987) and Kampunzu & Cailteux (1999), characterized by folding and thrusting with a northwards transport direction. This deformation stage which marks the paroxysm of the Lufilian shortening could have started earlier that the beginning of the first brittle stage, as discussed above.

Brittle deformations have been recorded in Manono in the Kibaran belt where they correspond to the earliest faulting in tin-bearing pegmatite dykes emplaced in Kibaran micaschists (Bernard, 1959). These dykes are related to post-orogenic Kibaran tin granitic intrusions, dated between 970 and 990 Ma in Rwanda (Tack et al., 2010), and for which a similar age has been obtained by S. Dewaele (personal communication) in the Kibaran belt. The earliest brittle fautling in Manono can therefore be coeval with the one observed in the Lufilian Arc.

The unfolding test suggests that the first brittle stage occurred before the arc bending, on a previously rectilinear belt trending obliquely to the direction of principal compression. The orientation of this rectilinear belt is not known, but normal to this trend lies at an average of 40° from the direction of compression. Using a NE (N140°E) pre-fautling trend, the average direction of compression in the Lufilian belt is restored to NNE-SSW (N11°E). This is close to the one obtained at Manono in the Kibaran belt which is supposed to have been unaffected by orogenic bending. With more E-W pre-brittle trends for the belt, restored compression direction would be in more westerly directions: a N120°E trend would give a N171°E compression and a N100°E trend, a N151°E compression. This last direction is highly oblique to the Manono reference, but close to the shortening directions in the NE-trending Luiro belt in Mozambique (Viola et al., 2008) and Damara belt in Namibia (Porada et al., 1983), as in the Namaqua basement of western South Africa (Viola et al., 2012). We relate this first brittle compression in the Lufilian arc, to the high-angle convergence between the Congo-Tanzania and Kalahari Cratons, in the frame of interactions between north and south Gondwana. More paleostress data outside the Lufilian arc needed to precise the original direction of compression.

Arc bending

The radial compression with variously oriented S_{Hmax} directions observed in the central part of the Lufilian arc (brittle stage 2) is interpreted as formed during the arc bending. It suggests constrictional tectonics and could be related to the formation of tectonic mega-breccia and related salt tectonics (Cailteux & Kampunzu, 1995; Jackson et al., 2003). The bending of the arc is expected to have generated local stress perturbations, limited to the hinge zone. Such constrictional deformation has not been observed elsewhere.

Lufilian transpression

The third brittle stage (NE-SW transpression) corresponds to the D2 or Monwezian deformation phase of François (1987) and Kampunzu & Cailteux (1999) which generated strike-slip movements in the already deformed folded and thrusted terranes. Our fault-kinematic data show that most minor fault planes are high angle, trending NE and with subhorizontal slip lines showing dominantly dextral strike-slip. It caused dextral strike-slip movements in the Kundelungu foreland, confined between the Bangweulu block and the Kibaran belt (Fig. 7c). Similar strike-slip movements also occurred inside the Kibaran belt as shown by the Manono data. In the NW-trending part of the Lufilian arc, it generated transversal, NE-trending fault zones that fragmented the ore deposits. The D2 – Monwezian stage is defined in the western part of the Lufilian arc by the E-W trending Monwezi fault system (François 1987), for which Kampunzu and Cailteux (1999) suggest left-lateral movements. This system fits well in a NE-SW transpressional context, the left-lateral E-W Monwezi fault system in the Lufilian arc and the right-lateral NE-SW faults of the Kundelungu foreland and Kibaran belt forming a conjugated fault system, both at an acute angle to the direction of principal compression.

The brittle stage 3 is further correlated with the first brittle deformation event recorded in the Ubende belt as thrust faulting regime under NE-SW compression (Delvaux et al., 2012). In the Ubende belt, it has been related to the interaction between the Tanzanian craton and the Bangweulu block during the late stage of the Pan-African assembly of Gondwana, after the last metamorphic overprint dated at 570 – 550 Ma (Boniface et al., 2012). The new data from the Lufilian arc agree well with this interpretation and further suggest a possible far-field effect of the collision of east and west Gondwana.

Relative timing of orogenic bending

Orogenic bending of the Lufilian belt has long been recognized to post-date the D1 -Kolwezian deformation stage. Our interpretation of the first brittle stage with the unfolding test agrees well with

this. Kampunzu & Cailteux (1999) propose that bending of the Lufilian arc occurred together with left-lateral movements along the Monwezi E-W fault system during the D2 - Monwezian stage. They explain this deformation as induced by an indenter in a similar way as India penetrating into Asia (Tapponnier et al., 1982). However, the stress directions of our third stress stage do not fit with the expected fan-shaped stress trajectories as seen in Asia (e.g. Flesch et al., 2001). They also do not seem to have been influenced by vertical-axis rotations as it would be the case if orogenic bending and strike-slip would be coeval. Finally, this bending occurs along the contact with the NE-trending Kibaran belt, with an expected right-lateral movement during our third stress stage. The polarity of the arc curvature is opposed to what could be expected if it was related to an interaction between the Lufilian and Kibaran belts. Therefore, we consider that the bending of the arc is a specific deformation stage that occurred between the D1 and D2 stages and is related to our second stress stage.

Late orogenic extension to extensional collapse

The brittle stage 4 marks the onset of late-orogenic extension in the Lufilian arc which reaches its full development during stage 5 by arc-parallel extension. They caused normal faulting reactivation of earlier compressional and strike-slip structures and induced new mineral remobilisations. These extensional

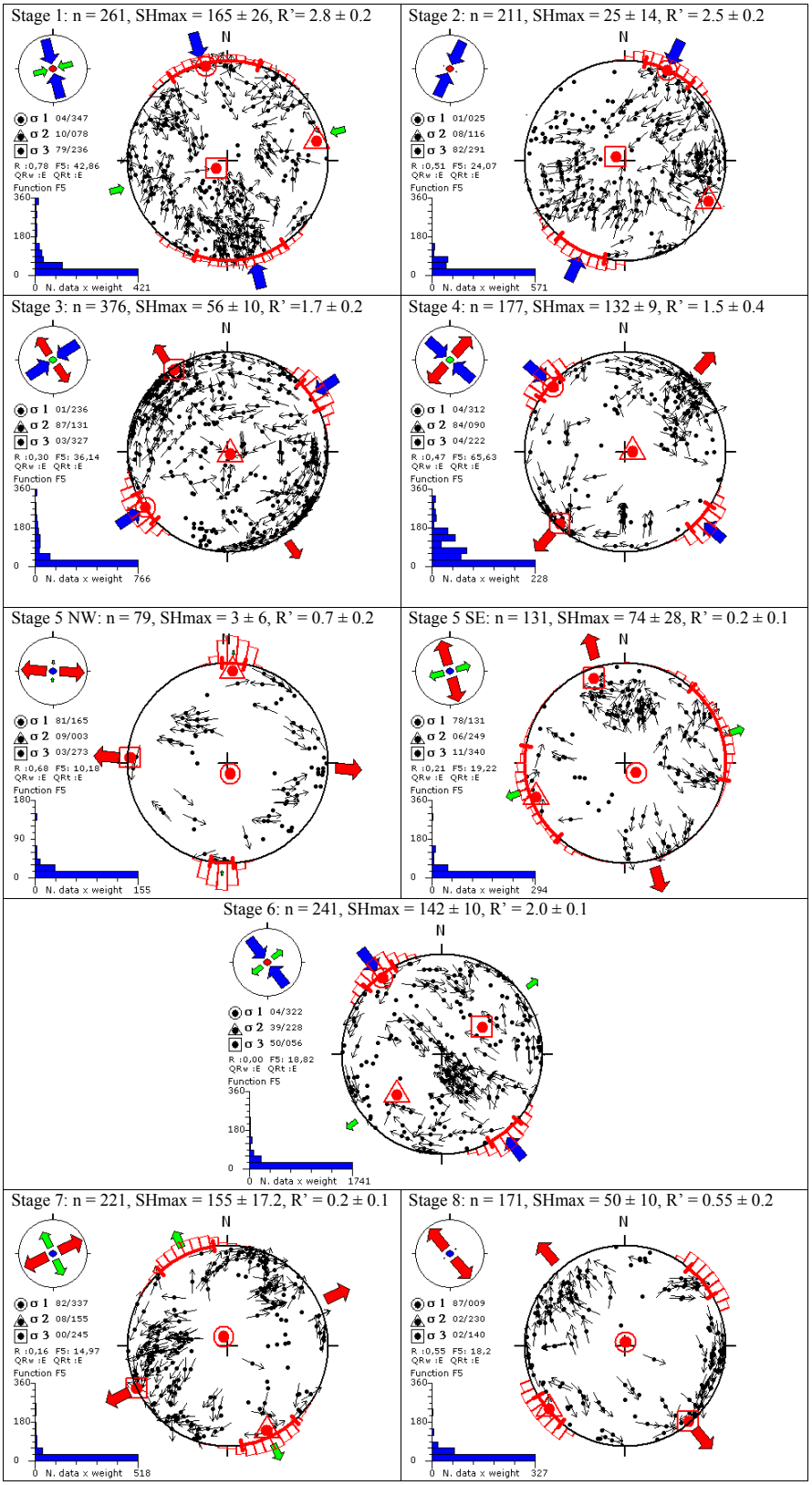

Figure 9. Average stress tensors for the 8 brittle stages obtained by the stress inversion of all the fault-slip data attributed the each stage (results in Table 3, lower lines). No additional separation was performed which explains the extreme values for the misfit function. Fault-slip data are displayed as tangent-lineation plot.

stages are recorded only in the Lufilian arc and therefore seem to be related to the geodynamic evolution of the arc itself. Stage 4 has a consistent NE-SW direction of extension across the arc, probably still controlled by a regional stress field. The arc parallel extension (stage 5) is entirely controlled by the structure of the arc, unrelated to plate dynamics as if the effects of the collision completely faded away. It can therefore be qualified as post-tectonic and could reflect gravitational collapse due to the action of arc-related gravitational instabilities at the end of the orogenic cycle.

Extensional collapse of orogens is known as a source for lithospheric extension along orogenic belts generated by body forces linked to isostatically compensated elevation and sharp elevation gradients (Dewey, 1988). Extension should have been initiated after the youngest age estimation of 530 Ma for the collisional process in the Lufilian arc (Porada & Behorst, 2000; John et al., 2004). It could be related to the vein-type deposits of Haest & Muchez (2011) which characterise the waning stage of the Lufilian orogeny. This late-to post-orogenic brittle extension could be coeval in the Luiro belt with the 530 - 507 Ma post-collisional magmatism and metamorphism evidended (Bingen et al., 2009) and the ductile extensional shear zones showing NE-SW crustal extension (Viola et al., 2008). The brittle stages 4 and 5 are therefore also interpreted as the result of orogenic collapse initiated by gravitational instabilities resulting from the crustal thickening of the shortening phase.

Early Mesozoic transpressional inversion

The NW-SE transpressional inversion recorded in the Lufilian arc as our brittle stage 6 affects also the Kundelungu Foreland (Dikulushi mine and Biano series of Pweto, Kat06), the Kibaran belt (Manono, Kat21) and the Ubende belt (Fig. 7f). It is therefore of regional importance, caused by external sources of stress unrelated to the Lufilian arc itself. It corresponds to the D3 – Shilatembo stage of Kampunzu & Cailteux (1999) and occurs after the Lufilian extensional collapse. In the Ubende belt, it affects Permian series (Delvaux et al., 2012). It can be further related to the post Permian but pre-late Jurassic structural inversion in the Congo basin (Daly et al., 1992; Kadima et al., 2011), post-Karoo (eq. Beaufort Group) middle Triassic inversions in the Luangwa basin in Zambia (Banks et al., 1995), Ruhuhu basin in SW Tanzania (unpublished observations of D. Delvaux) and to the Waterberg thrust in Namibia that brought the Precambrian basement over the Triassic Waterberg series (Miller, 2008). It could also correspond to the middle Triassic stratigraphic hiatus between the Beaufort and the Stormberg Groups in the Karoo Supergroup of South Africa (Catuneanu et al., 2005).

The observed transpressional inversion and the other coeval compressional deformations reported in sub-equatorial Africa for the late Permian - Triassic period are considered as the result of far-field stresses related to the Gondwanide passive margin orogen at the southern margin of the Gondwana continent, expressed in South Africa by the Cape Fold Belt (e.g. Johnston, 2000). Although not precisely constrained in age, this transpressional inversion appears too old to represent the late Santonian (85-83 Ma) or late Maastrichtian (69-65 Ma) regional inversion events that have been reported in many African basins north of the Equator (Guiraud & Bosworth, 1997; Bosworth et al., 1999) and also in south-western Africa (Viola et al., 2012).

Rift-related extension

After the early Mesozoic inversion, the Lufilian arc and the surrounding areas entered in a long period dominated by extensional tectonics related to the Mesozoic breakup of Gondwana and the Cenozoic East African rifting. The well-expressed brittle stage 7 with NNE-SSW to NE-SW extension is related the development of the Tanganyika rift trend. Stage 8 represents rifting under NNW-SSE extension (Moero-Upemba rift trend) and is compatible with present-day extension as constrained by earthquake focal mechanisms. The spatially and temporally changing stress field can be explained by the interaction of differently oriented rift branches, all of them characterized by orthogonal opening: the NW-trending southern part of the Tanganyika rift and the NE-trending Moero graben (Delvaux & Barth, 2010). The slight transpressional component observed for stage 8 is explained by the spatial transition from NE-SW extension in the Rukwa and Tanganyika rift basins to the NW-SE extension in the Moreo-Upemba region.

9. Conclusion

This study has provided a large set of brittle structures and their fault-kinematic analysis and paleostress reconstructions allow for the first time an insight into the brittle tectonic evolution of the Lufilian belt since the paroxysm of the Lufilian orogeny. The integration of new and published data from adjacent regions (Kundelungu foreland, Kibaran and Ubende belts) provides a regional dimension to the results and conclusions. The Central African region of the Lufilian belt endured a long-lasting and complex brittle evolution that was influenced by both locally generated and plate-scale processes. The fluctuation of tectonic stresses trough time reflects several first-order geodynamic events that affected a much wider region than the one investigated. The brittle data illustrate several stages of deformation related to the Lufilian orogeny, since the onset of the brittle realm, at about 550 Ma ago, from the paroxysm of orogenic compression to the orogenic collapse. A second geodynamic event was recorded as a transpressional inversion which is interpreted as a far-field effect of the Cape fold belt of the Gondwanide orogeny during early Mesozoic. The effects of the widely recognised late Santonian and late Maastrichtian regional inversion events have not been found. After this early Mesozoic inversion, Lufilian region entered in an extensional setting related to the breakup of Gondwana. It is not clear when the extensional conditions started, but two major directions of extension apparently succeeded in time, with the last one fitting the current extension directions deduced from earthquake focal mechanisms.

Acknowledgements

This work is a scientific output of the Framework Agreement MRAC-DGCD project S1_RDC_GEODYN_UNILU. Louis Kipata is supported by a Mixt PhD grant from the Belgium Cooperation. Damien Delvaux is working under Belspo Action 1 projects. The authors thank the mining companies that provided access to their deposits for field investigations (GECAMINES, Forrest Group, First Quantum Minerals, Boss Mining, CIMENKAT, CHEMAF, SODIMICO). S. Vandyke and G. Viola are thanked for their reviewing and constructive remarks.

References

Angelier, J. 1989. From orientation to magnitudes in paleostress determinations using fault slip data. Journal of Structural Geology, 11, 37-50.

Angelier, J., 1994. Fault slip analysis and paleostress reconstruction. in: P.L. Hancock (ed.) Continental Deformation, Pergamon, Oxford, 101-120.

Angelier, J. & Manoussis, S., 1980. Classification automatique et distinction de phases superposées en tectonique cassante. C. R. Acad. Sci. Paris, D290, 651-654.

Banks, N.L., Bardwell, K.A., Musiwa, S., 1995. Karoo rift Basins of the Luangwa Valley, Zambia. In: Lambiase, J.J. (Ed.), Hydrocarbon Habitat in Rift Basins, Geological Society Special Publication, 80, 285-295.

Batumike, J.M., Griffin, W.L., Belousova, E.A., Pearson, N.J., O'Reilly, S.Y. & Shee, S.R., 2008. LAM-ICPMS U-Pb dating of kimberlitic perovskite: Eocene-Oligocene Kimberlites from the Kundelungu Plateau, D.R. Congo. Earth and Planetary Science Letters, 267(2008), 609-619.

Batumike, M.J., Cailteux, J.L.H. & Kampunzu, A.B., 2007. Lithostratigraphy, basin development, base metal deposits, and regional correlations of the Neoproterozoic Nguba and Kundelungu rock successions, central African Copperbelt. Gondwana Research, 11(3), 432-447.

Bernard, H., 1954. Quelques observations sur des filons zonaires pegmatitiques à Manono. Annales de la Société géologique de Belgique, 78, 41-50.

Bingen, B., Jacobs, J., Viola, G., Henderson, I.H.C., Skår, Ø., Boyd, R., Thomas, R.J., Solli, A., Key, R.M., Daudi, E.X.F., 2009. Geochronology of the Precambrian crust in the Mozambique belt in NE Mozambique, and implications for Gondwana assembly. Precambrian Research, 170(3-4), 231-255.

Boniface, N., Schenk, V. & Appel, P., 2012. Paleoproterozoic eclogites of MORB-type chemistry and three Proterozoic orogenic cycles in the Ubendian Belt (Tanzania): Evidence from monazite and zircon geochronology, and geochemistry. Precambrian Research, 192-193, 16-33.

Bosworth, W., Guiraud, R.A. & Kessler, L.G., 1999. Late Cretaceous (ca. 84 Ma) compressive deformation of the stable platform of northeast Africa (Egypt): Far-field stress effects of the Santonian event and origin of the Syrian arc deformation belt. Geology, 27(7), 633-636.

Bott, M.H.P., 1959. The mechanisms of oblique slip faulting. Geological Magazine, 96, 109-117.

Buffard, R., 1988. Un rift intracontinental du Précambrien supérieur : Le Shaba méridional (Zaire). Thèse de doctorat d'état es sciences, University of Maine, France, 316p.

Cahen, L., 1954. La géologie du Congo Belge. Vaillant H. Carmanne, Liège, 577p.

Cailteux, J., 1994. Lithostratigraphy of the Neoproterozoic Shaba-type (Zaïre) Roan Supergroup and metallogenesis of associated stratiform mineralisation. Journal of African Earth Sciences, 19, 279–301.

Cailteux, J.L.H. & Kampunzu, A.B., 1995. The Katangan tectonic breccias in the Shaba Province (Zaire) and their genetic significance. Annales des Sciences Géologiques, Royal Museum of Central Africa, 101, 63-76.

Cailteux, J.L.H., Kampunzu, A.B. & Lerouge, C., 2007. The Neoproterozoic Mwashya-Kansuki sedimentary rock succession in the central African Copperbelt, its Cu-Co mineralisation, and regional correlations. Gondwana Research, 11(3), 414-431.

Cailteux, J.L.H., Kampunzu, A.B.H. & Batumike, M.J., 2005a. Lithostratigraphic position and petrographic characteristics of R.A.T. ("Roches Argilo-Talqueuses") Subgroup, Neoproterozoic Katangan Belt (Congo). Journal of African Earth Sciences, 42, 82-94.

Cailteux, J.L.H., Kampunzu, A.B., Lerouge, C., Kaputo, A.K. & Milesi, J.P., 2005b. Genesis of sediment-hosted stratiform copper-cobalt deposits central African Copperbelt. Journal of African Earth Sciences, 42, 134-158.

Cailteux, J.L.H. & Misi, A., 2007. Neoproterozoic sediment-hosted base metal deposits of Western Gondwana. Gondwana Research, 11(3), 344-345.

Calais, E., C., Ebinger, C., Hartnady & Nocquet, J.M., 2006. Kinematics of the East African Rift from GPS and earthquake slip vector data. Geological Society of London, Special Publications, 259, 9-22.

Carey-Gailhardis, E. & Mercier, J.-L., 1987. A numerical method for determining the state of stress using focal mechanisms of earthquake populations: Application to Tibetan teleseisms and microseismicity of southern Peru. Earth and Planetary Science Letters, 82, 165-179.

Catuneanu, O., Wopfner, H., Eriksson, P.G., Cairncross, B., Rubidge, B.S., Smith R.M.H. & Hancox, P.J., 2005. The Karoo basins of south-central Africa. Journal of African Earth Sciences, 43, 211-253.

Craig, T.J., Jackson, J.A., Priestley, K. & McKenzie, D., 2011. Earthquake distribution patterns in Africa: their relationship to variations in lithospheric and geological structure, and their rheological implications. Geophysical Journal International, 185(1), 403-434.

Daly, M.C., Chakraborty, S.K., Kasolo, P., Musiwa, M., Mumba, P., Naidu, B., Namateba, C., Ngambi, O. & Coward, M.P., 1984. The Lufilian arc and Irumide belt of Zambia: results of a traverse across their intersection. Journal of African Earth Science, 4, 311-318.

Daly, M.C., Lawrence, S.R., Diemu-Tshiband, K. & Matouana, B., 1992. Tectonic evolution of the Cuvette Centrale, Zaire. Journal of the Geological Society, London, 149(4), 539–546.

De Putter, T., Mees, F., Decrée, S. & Dewaele, S., 2010. Malachite, an indicator of major Pliocene Cu remobilization in a karstic environment (Katanga, Democratic Republic of Congo). Ore Geology Reviews, 38(1-2), 90-100.

De Swardt, A.M.J. & Drysdall, A.R., 1964. Precambrian geology and structure in central Northern Rhodesia. Geological Survey of Northern Rhodesia Memoir 2, 82.

De swardt, A.M.J., Garrard, P. & Simpson, J.G., 1965. Major zones of transcurrent dislocation and superimposition of orogenic belts in part of central Africa. Bull. Geol. Soc. Am., 76, 89-102.

De Waele, B., Johnon, S.P. & Pisarevsky, S.A., 2008. Paleoproterozoic to Neoproterozoic growth and evolution of the eastern Congo Craton: Its role in the Rodinia puzzle. Precambrian Research, 160, 127-141.

Delvaux, D., 2012. Release of program Win-Tensor 4.0 for tectonic stress inversion: statistical expression of stress parameters. EGU General Assembly, Vienna, 2012. Geophysical Research Abstracts, Vol. 14, EGU2012-5899. Program available at http://users.skynet.be/damien.delvaux/Tensor/tensor-index.html.

Delvaux, D. & Barth, A., 2010. African stress pattern from formal inversion of focal mechanism data. Tectonophysics, 482, 105-128.

Delvaux, D., Kervyn, F., Macheyeki, A.S. & Temu, E.B., 2012. Geodynamic significance of the TRM segment in the East African Rift (W-Tanzania): active tectonics and paleostress in the Ufipa plateau and Rukwa basin. Journal of Structural Geology, 37, 161-180.

Delvaux, D., Moeys, R., Stapel, G., Petit, C., Levi, K., Miroshnichenko, A., Ruzhich, V. & Sankov, V., 1997. Paleostress reconstructions and geodynamics of the Baikal region, Central Asia. Part II: Cenozoic rifting. In: Cloetingh, S., Fernandez, M., Munoz, J.A., Sassi, W., & Horvath, F. (eds), Structural controls on sedimentary basin formation. Tectonophysics, 282, 1-38.

Delvaux, D. & Sperner, B., 2003. Stress tensor inversion from fault kinematic indicators and focal mechanism data: the TENSOR program. Geological Society of London, Special Publications, 212, 75-100.

Dewaele, S., Muchez, P., Vets, J., Fernandez-Alonzo, M. & Tack, L., 2006. Multiphase origin of the Cu-Co ore deposits in the western part of the Lufilian fold-and-thrust belt, Katanga (Democratic Republic of Congo). Journal of African Earth Sciences, 46(5), 455-469.

Dewey, J.F., 1988. Extensional collapse of orogens. Tetonics, 7(6), 1123-1139.

Dunne, W.M. & Hancock, P.L. 1994. Paleostress analysis of small-scale brittle structures. In: Hancock, P.L. (ed.) Continental Deformation. Pergamon, Oxford, 101-120.

El Desouky, H., Muchez, Ph., Boyce, A.J., Schneider, J., Cailteux, J., Dewaele, S. & von Quadt, A, 2010. Genesis of sediment-hosted stratiform copper–cobalt mineralization at Luiswishi and Kamoto, Katanga Copperbelt (Democratic Republic of Congo). Mineralium Deposita, 45(8), 735-763.

El Desouky, H.A., Muchez, P. & Cailteux, J., 2009. Two Cu-Co sulfide phases and contrasting fluid systems in the Katanga Copperbelt, Democratic Republic of Congo. Ore Geology Reviews, 36(4), 315-332.

Flesch, L.M., Haines, A.J. & Holt, W.E., 2001. Dynamics of the India-Eurasia collision zone. Journal of Geophysical Research, 106(B8), 16435-16460.

François, A., 1987. Synthèse géologique sur l'arc cuprifère du Shaba (Rép. du Zaïre). Centenaire de la Société Belge de Géologie, 15–65.

François, A., 1993. La structure tectonique du Katangien dans la région de Kolwezi (Shaba, Rep. Du Zaïre). Annales Société géologique de Belgique 116(1), 87-104.

François, A., 2006. La partie centrale de l'arc cuprifère du Katanga: étude géologique. Tervuren African Geoscience Collection, 109, 61p.

Frimmel, H., Tack, L., Basei, M., Nutman, A. & Boven, A., 2006. Provenance and chemostratigraphy of the Neoproterozoic West Congolian Group in the Democratic Republic of Congo. Journal of African Earth Sciences, 46, 221-239.

Frimmel, H.E., Basei, M.S. & Gaucher, C., 2011. Neoproterozoic geodynamic evolution of SW-Gondwana: a southern African perspective. International Journal of Earth Sciences, 100(2-3), 323-354.

Gephart, J.W. & Forsyth, D.W., 1984. An improved method for determining the regional stress tensor using earthquake focal mechanism data: Application to the San Fernando earthquake sequence. Journal of Geophysical Research, 89, 9305-9320.

Grantham, G.H., Maboko, M. & Eglington, B.M., 2003. A Review of the Evolution of the Mozambique Belt and Implications for the Amalgamation and Dispersal of Rodinia and Gondwana. Geological Society of London, Special Publications, 206, 401-425.

Guiraud, R. & Bosworth, W., 1997. Senonian basin inversion and rejuvenation of rifting in Africa and Arabia: Synthesis and implications to plate-scale tectonics. Tectonophysics, 282, 39–82.

Haest, M., 2009. Metallogenesis of the Dikulushi Cu-Ag deposit in Katanga (DRC). Katholieke Universiteit Leuven, Belgium, Ph.D. thesis. Aardkundige Mededelingen, 17, 238p..

Haest, M. & Muchez, 2011. Stratiform and vein-type deposits in the Pan-African orogen in Central and Southern Africa: Evidence for multiphase mineralisation. Geologica Belgica, 14(1-2), 23-44.

Haest, M., Muchez, P., Dewaele, S., Franey, N., Tyler, R., 2007. Structural control of the Dikulushi Cu-Ag deposit, Katanga, Democratic Republic of Congo. Economic Geology, 102, 1321-1333.

Haest, M., Muchez, P., Dewaele, S., Schneider, J. & Boyce, A.J., 2009. Petrographic, fluid inclusion and isotopic study of the Dikulushi Cu–Ag deposit, Katanga (D.R.C.): implications for exploration. Mineralium Deposita, 44(5), 505-522.

Haest, M., Schneider, J., Cloquet, C., Latruwe, K., Vanhaecke, F. & Muchez, P., 2010. Pb isotopic contraints on the formation of the Dikulushi Cu-Pb-Zn-Ag mineralisation, Kundelungu Plateau (Democratic Republic of Congo). Mineralium Deposita, 45, 393-410.

Hanson, R.E., Wardlaw, M.S., Wilson, T.J. & Mwale, G., 1993. U-Pb zircon ages from the Hook granite massif and Mwembeshi dislocation: constraints on Pan-African deformation, plutonism, and transcurrent shearing in central Zambia. Precambrian Research, 63, 189-206.

Jackson, M.P.A., Warin, O.N., Woad, G.M. & Hudec, M.R., 2003. Neoproterozoic allochthonous salt tectonics during the Lufilian orogeny in the Katangan Copperbelt, central Africa. Bull. Geol. Soc. Am., 115(3), 314-330.

Jacobs, J., Bingen, B., Thomas, R.J., Bauer, W., Wingate, M.T.D. & Feitio, P., 2008. Early Palaeozoic orogenic collapse and voluminous late-tectonic magmatism in Dronning Maud Land and Mozambique: insights into the partially delaminated orogenic root of the East African–Antarctic Orogen? Geological Society of London, Special Publications, 308, 69-90.

John, T., Schenk, V., Mezger, K. & Tembo, F., 2004. Timing and PT evolution of whiteschist metamorphism in the Lufilian Arc - Zambezi belt orogen (Zambia): implications for the assembly of Gondwana. Journal of Geology, 112, 71-90.

Johnston, S.T., 2000. The Cape Fold Belt and Syntaxis and the rotated Falkland Islands: dextral transpressional tectonics along the southwestern margin of Gondwana. Journal of African Earth Sciences, 31, 51-63.

Kadima, E., Delvaux, D., Sebagenzi, S.N., Tack, L. & Kabeya, M., 2011. Structure and geological history of the Congo Basin: An integrated interpretation of gravity, magnetic and reflection seismic data. Basin Research, 23(5), 499-527.

Kampunzu, A.B. & Cailteux, J.L.H., 1999. Tectonic evolution of the Lufilian Arc (Central Africa Copper Belt) during Neoproterozoic Pan African orogenesis. Gondwana Research, 2(3), 401-421.

Kampunzu, A.B., Cailteux, J.L.H., Kamona, A.F., Intiomale, M.M. & Melcher, F., 2009. Sediment-hosted Zn-Pb-Cu deposits in the Central African Copperbelt. Ore Geology Reviews, 35(3-4), 263-297.

Kampunzu, A.B., Kanika, M., Kapenda, D. & Tshimanga, K., 1993. Geochemistry and geotectonic evolution of late Proterozoic Katangan basic rocks from the Kibambale in central Shaba (Congo). Geologisch Rundschau, 82, 619–630.

Kampunzu, A.B., Tembo, F., Matheis, G., Kapenda, D. & Huntsman-Mapila, P., 2000. Geochemistry and tectonic setting of mafic igneous units in the Neoproterozoic Katangan Basin, Central Africa: Implication for Rodinia break up. Gondwana Research, 3, 125–153.

Kazadi, B., 2012. Structural geology of the Kinsevere Copper Deposit. Ms.C Thesis, University of Pretoria, South-Africa.

Kinabo, B.D., Atekwama, E.A., Hogan, J.P., Modisi, M.P., Wheaton, D.D. & Kampunzu, A.B., 2007. Early development of the Okavango rift zone, NW Botswana. Jounrla of African Earth Sciences, 48, 125-136.

Kipata, M.L., 2007. Inventaire et analyse au moyen d'un SIG de la tectonique active dans le SE de l'Afrique: Sud-est de la RDC et Nord de la Zambie. MSc. thesis, Faculteit Wetenschappen, K.U.Leuven, Belgium, 106pp.

Kokonyangi, J.W., Kampunzu, A.B., Armstrong, R., Yoshida, M., Okudaira, M., Arima, M. & Ngulube, D.A., 2006. The Mesoproterozoic Kibaride belt (Katanga, SE D.R. Congo). Journal of African Earth Sciences, 46(1-2), 1-35.

Kounov, A., Burg, J.-P., Bernouilli, D., Seward, D., Ivanov, Z., Dimov, D. & Gerdjikov, I., 2011. Paleostress analysis of Cenozoic faulting in the Kraishte area, SW Bulgaria. Journal of Structural geology, 33, 859-874.

Kröner, A., Willner, H.P., Hegner, E., Jaeckel, P. & Nemchin, A., 2001. Single zircon ages, PT evolution and Nd isotope systematics of high-grade gneisses in southern Malawi and their bearing on the evolution of the Mozambique Belt in southeastern Africa. Precambrian Research, 109, 257–291.

Lacombe, O., 2012. Do slip data inversions actually yield « paleostress » that can be compared with contemporary stresses ? A critical discussion. Compte Rendu Geosciences, 344, 159-173.

Lund, B. & Townend, J., 2007. Calculating horizontal stress orientations with full or partial knowledge of the tectonic stress tensor. Geophysical Journal International, 270, 1328-1335.

Marett, R.A. & Allmendinger, R.W., 1990. Kinematic analysis of fault-slip data. Journal of Structural Geology, 12, 973-986.

Meert, J.G. & Van der Voo, R., 1997. The assembly of Gondwana 800–550 Ma. Journal of Geodynamics, 23, 223–235.

Mendelsohn, F., 1961. The Geology of the Northern Rhodesian Copperbelt. Macdonald, London, 523p.

Michael, A.J., 1984. Determination of stress from slip data: faults and folds. Journal of Geophysical Research, 89(B13), 11517–11526.

Miller, R.McG., 2008. The Geology of Namibia. Volume 3. Geological Survey of Namibia, Windhoek.

Mondeguer, A., Ravenne, C., Masse, P. & Tiercelin, J.-J., 1989. Sedimentary basin in an extension and strike-slip background : the « South Tanganyika troughs complex", East African Rift. Bull. Soc. Geol. France, 8, V, 501-522.

Muchez, P., Brems, D., Clara, E., De Cleyn, A., Lammens, L., Boyce, A., De Muynck; D., Mukumba & Sikaswe, O., 2010. Evolution of Cu-Co mineralizing fluids at Nkana Mine, Central African Copperbelt, Zambia. Journal of African Earth Sciences, 58(3), 457-474.

Muchez, P., Vanderhaeghen, P., El Desouky, H., Schneider, J., Boyce, A., Dewaele, S. & Cailteux, J., 2008. Anhydrite pseudomorphs and the origin of stratiform Cu–Co ores in the Katangan Copperbelt (Democratic Republic of Congo). Mineralium Deposita, 43(5), 575-589.

Oosterbosch, R., 1962. Les minéralisations dans le système de Roan au Katanga. In: Lombard, J., Nicolini, P. (eds), Gisements Stratiformes de Cuivre en Afrique, 1ère Partie. Association des Services Géologiques Africains, Paris 71–136.

Petit, J.P., 1987. Criteria for the sense of movement on fault surfaces in brittle rocks. Journal of Structural Geology, 9, 597-608.

Petit, C., Deverchère, J., Houdry-Lémont, F., Sankov, V.A., Melnikova, V.I. and Delvaux, D., 1996. Present-day stress field changes along the Baikal rift and tectonic implications. Tectonics, 15(6), 1171-1191.

Porada, H. & Berhorst, V., 2000. Towards a new understanding of the Neoproterozoic-Early Palaeozoic Lufilian and northern Zambezi Belts in Zambia and the Democratic Republic of Congo. Journal of African Earth Sciences, 30(3), 727-771.

Robert, 1956. Géologie et Géographie du Katanga y compris l'étude des ressources et de la mise en valeur. Hayez, Bruxelles, 620p.

Scholz, C.H., Koczynski, T.A. & Hutchins, D.G., 1976. Evidence for incipient rifting in Southern Africa. Geophys. J. R. astr. Soc., 44, 135-144.

Sebagenzi, M.N. & Kaputo, A.K., 2002. Geophysical evidences of continental break up in the southeast of the Democratic republic of Congo and zambia (Central Africa). EGU Stephan Mueller Spec. Publ. Series, 2(2002), 193-206.

Shackleton, R.M., 1994. The final collision zone between East and West Gondwana; where is it? Journal of African Earth Sciences, 23, 271-287.

Sperner, B., Ratschbacher, L. & Ott, R., 1993. Fault-striae analysis: A Turbo-Pascal program package for graphical presentation and reduced stress tensor calculation. Computer and Geosciences, 19, 1361-1388.

Tack, L., Wingate, M.T.D., De Waele, B., Meert, J., Belousova, E., Griffin, B., Tahon, A., Fernandez-Alonso, M., 2010. The 1375 Ma "Kibaran event" in Central Africa: Prominent emplacement of bimodal magmatism under extensional regime. Precambrian Research, 180(1-2), 63-84

Tapponnier, P., Peltzer, G., Le Dain, A.Y., Armijo ; R. & Cobbold, P., 1982. Propagating extrusion tectonics in Asia : New insights from simple experiments with plasticine. Geology, 10(12), 611-616.

Tembo, F., Kampunzu, A.B. & Porada, H., 1999. Tholeiitic magmatism associated with continental rifting in the Lufilian Fold Belt of Zambia. Journal of African Earth Sciences, 28, 403–425.

Tshiauka, T., Katekesha, W.M., Cailteux, J., Intiomale, M.M., Kampunzu, A.B., Kapenda, D., Chabu, M., Ngongo, K., Mutombo, K., & Nkanika, W.R., 1995. Lithostratigraphy of the NeoProterozoic Katangan sedimentary sequences in the Musoshi Copper District (SE Shaba, Zaire) and incidences on copper and cobalt economic geology in Central Africa. Annales Musée royal Afrique centrale, Tervuren (Belgique), série in-8, Sciences géologiques, 101, 29–48.

Unrug, R., 1988. Landsat-based structural map of the Lufilian fold belt and the Kundelungu aulacogene, Shaba (Zaire), Zambia ad Angola, and the regional position of Cu, Co, U, Au, Zn and Pb mineralisation. Geological Association of Canada, Special Paper, 36, 519-524.

Vandycke, S. & Bergerat, F., 1992. Tectonique de failles et paléo-contraintes dans les formations crétacées du Boulonnais (France). Implications géodynamiques. Bulletin de la Société géologique de France, 163(5), 553-560.

Viola, G., Henderson, I. H. C., Bingen, B., Thomas, R. J., Smethurst, M. A. & de Azavedo, S., 2008. Growth and collapse of a deeply eroded orogen: Insights from structural, geophysical, and geochronological constraints on the Pan-African evolution of NE Mozambique. Tectonics, 27, TC5009.

Viola, G., Kounov, A., Andreoli, M. and Mattila, J., 2012. Brittle tectonic evolution along the western margin of South Africa: more than 500 Myr of continued reactivation. Tectonophysics, 514-517, 93-114.

Viola, G., Venvik Ganerød G. & Wahlgren, C.-H., 2009. Unravelling 1.5 Gyr of brittle deformation history in the Laxemar-Simpevarp area, SE Sweden: a contribution to the Swedish site investigation study for the disposal of highly radioactive nuclear waste. Tectonics, 28, TC5007.

Wallace, R.E., 1951. Geometry of shearing stress and relation to faulting. Journal of Structural Geology, 59, 118-130.

Wendorff, M., 2011. Tectonosedimentary expressions of the evolution of the Fungurume foremand basin in the Lufilian Arc, Neoproterozoic-Lower Palaeozoic, Cerntral Africa. Geological Society of London, Special Publications, 357, 69-83.

Westerhof, A.B.P., Lehtonen, M.I., Mäkitie, H., Manninen, T., Pekkala, Y., Gustafsson, B. & Tahon, A., 2008. The Tete-Chipata Belt: A new multiple terrane element from western Mozambique and southern Zambia. Geological Survey of Finland Special Paper 48, 145–166.

Wilson, T., Grunow, A. M. & Hanson, R. E., 1997. Gondwana assembly: The view from southern Africa and East Gondwana. Journal of Geodynamics, 23, 263–286.

Manuscript received 24.10.2011, accepted in revised form 29.06.2012, available on line 15.11.2012